https://doi.org/10.5194/egusphere-2026-4720
Preprint. Discussion started: 14 August 2026
© Author(s) 2026. CC BY 4.0 License.

Methodological Framework for Tsunami Risk Assessment in Port Facilities

Sergio Padilla[1], Ignacio Aguirre-Ayerbe[1], Mauricio González[1], Íñigo Aniel-Quiroga[2], David Galán Pérez[1]

[1]IHCantabria - Instituto de Hidráulica Ambiental de la Universidad de Cantabria, Santander, Spain
[2]IDOM, Consulting, Engineering, Architecture – Avda. Zarandoa 23, 48015, Bilbao, Bizkaia, Spain

Correspondence to: Sergio Padilla (padillas@unican.es)

Abstract. The present study proposes a comprehensive methodological framework for the assessment of tsunami risk in port terminals. Although tsunami hazard modeling has advanced significantly, the development of asset-specific vulnerability functions and risk indicators at the terminal scale remains a critical challenge, hindering the effective integration of scientific knowledge into operational port planning. The main objective of this study is to propose a methodological framework specifically tailored to tsunami risk assessment in port terminals. The analysis focuses on assessing damage to key components of the port supply chain located within the port's landside operational area and directly exposed to tsunami impacts. The proposed framework integrates advanced numerical hydrodynamic modeling, dynamic exposure analyses and asset-specific damage states. Its main novelty lies in the quantification of vulnerability thresholds based on hydrodynamic failure mechanisms for heterogeneous port assets, including container stacks, gantry cranes, liquid bulk tanks, Ro-Ro, and pedestrians. The methodology was applied to the Port of Cádiz, Spain. The results show that relative tsunami risk is spatially concentrated in specific operational areas and assets, particularly container storage yards and passenger circulation zones. The proposed framework is modular and can be adapted to other port contexts, provided that suitable local hazard, exposure, and asset information is available. Rather than providing absolute estimates of losses, the framework offers a spatially explicit decision-support basis for identifying critical assets, comparing relative risk among docks, and prioritising further detailed assessments or mitigation actions.

1. Introduction

Ports are complex critical infrastructures that concentrate economic assets, logistics activities, and human presence in highly exposed coastal environments. While tsunami hazard has been extensively studied from a geophysical and coastal engineering perspective, its integration into asset-focused, integrated risk assessments at the scale of port terminals remains limited.

Port facilities are vital nodes in the global supply chain and pillars of the global economy. They serve as essential hubs for trade and logistics and facilitating 80% of world trade by volume (Notteboom et al., 2021). A port area is designed to facilitate port and logistics operations related to maritime transport and its interconnection with other modes of transport and with comprehensive ship management, including operations related to nautical-sporting, industrial, and military activities (Puertos

https://doi.org/10.5194/egusphere-2026-4720
Preprint. Discussion started: 14 August 2026
© Author(s) 2026. CC BY 4.0 License.

Del Estado, 2001). Due to their location in coastal areas, these infrastructures are intrinsically vulnerable to extreme marine events, with tsunamis being one of the most destructive threats.

Tsunamis, as high-impact, low-probability events, are often underestimated or ignored in risk management planning and have not been studied in detail in the context of port engineering (Borrero et al., 2015). Despite the existence of studies addressing the impact of tsunamis on ships (Muhari et al., 2015; Padilla et al., 2024), damage to marina docks (Keen et al., 2017, 2021), and container behaviour under tsunami loading (Hwang et al., 2023; Lee et al., 2024), these efforts remain largely fragmented, highlighting the need for an integrated assessment at the scale of the port system. This situation has been linked to a broader disconnection between scientific knowledge on tsunami hazards and its incorporation into routine port planning and risk management practices.

Although tsunami hazard modelling has advanced substantially, its translation into asset-level risk information for port terminals remains limited. Existing studies often address individual components, such as vessels, marinas, cranes, or containers, but rarely integrate hazard, exposure, and vulnerability within a spatially explicit framework suitable for port management. This limitation restricts the consistent translation of scientific knowledge into structured decision-support tools for port risk management.

Historically, multiple devastating tsunamis have severely impacted port facilities across the globe. One of the most vivid examples of tsunami damage to maritime infrastructure is the 1868 Arica tsunami, in which more than 212 men from 16 vessels anchored in Arica perished. Another event is the 2010 Maule tsunami, triggered by an 8.8 magnitude earthquake, which caused significant damage to Chilean coastal infrastructure (Borrero et al., 2015). The 2006 Kuril Islands Tsunami, despite being a moderate event across the Pacific, caused substantial damage with estimated losses of US$1 million at the Crescent City marina in California (Kelly et al., 2006). Another significant incident occurred in January 2022, when an oil tanker located in Puerto La Pampilla (Perú), broke its moorings due to a volcanic meteorological tsunami and spilled more than 11,000 barrels of crude oil along the coast of Peru (Padilla et al., 2024), causing an ecological disaster in the country.

The 2011 Tohoku earthquake and tsunami, however, stands out as a particularly notable event in port environments (Chua et al., 2021; Hatayama, 2015; Suppasri et al., 2012; Tomita et al., 2013; Wilson et al., 2013). The Ministry of Agriculture, Forestry and Fisheries published a report stating that 319 ports and approximately 1,725 marine facilities were damaged by the tsunami, which brought economic losses of approximately US$12 billion (Muhari et al., 2015).

The latter promoted the development of the first comprehensive database of tsunami damage specifically for port industries and related structures, which has been decisive for estimating tsunami damage to port infrastructure (Takahashi et al., 2014).

The vital economic function of ports alongside their fragility in the event of tsunamis poses a significant challenge. A framework for risk management and tsunami impact planning is required to proactively identify and assess vulnerabilities (Wannous and Velasquez, 2017). Therefore, there is a need for an integrated tsunami risk assessment methodology that goes beyond simplistic flood depth analysis to encompass the complexities of hydrodynamic interactions and port superstructure vulnerability. This is precisely the scope of this work.

https://doi.org/10.5194/egusphere-2026-4720
Preprint. Discussion started: 14 August 2026
© Author(s) 2026. CC BY 4.0 License.

The main objective of this study is to propose a methodological framework specifically tailored to tsunami risk assessment in port terminals. This analysis focuses on assessing damage to key components of the port supply chain located within the port's landside operational area and directly exposed to tsunami impacts. These assets include cargo-handling equipment (e.g., cranes), storage facilities (such as office buildings and warehouses), storage tanks, goods (containerized, Lo-Lo, and Ro-Ro), and people.

This study contributes to addressing this gap by proposing a structured methodological framework for assessing tsunami risk in port facilities, explicitly linking hazard, exposure, and asset-specific fragility and vulnerability through spatial aggregation at dock-level. The proposed methodology is designed to be replicable and applicable in port risk management contexts, enabling the identification of high-risk areas and supporting the prioritisation of resilience and mitigation measures. This integrated approach addresses limitations in previous studies that focused exclusively on structural vulnerability or lacked spatial aggregation frameworks applicable at the scale of port terminals.

This paper is structured as follows: first, the proposed methodological framework for tsunami risk assessment in port environments is outlined. The main components of the framework are then described, including port characterization, tsunami hazard assessment, and asset-specific fragility and vulnerability evaluation, which are subsequently integrated through a dock-level risk aggregation approach. Finally, the applicability of the methodology is illustrated through a case study at the Port of Cádiz, Spain.

2. Methodological framework for assessing tsunami risk to port facilities

This section presents the conceptual and methodological framework adopted for tsunami risk assessment in port facilities. Risk is defined in terms of hazard, exposure, and vulnerability, with an explicit focus on direct physical impacts on port assets at terminal and dock scales. The framework provides a structured basis for integrating tsunami hazard assessment, asset exposure, and fragility-based vulnerability within a coherent risk assessment approach applicable to complex port environments (see Figure 1).

The methodology begins with a comprehensive characterisation of the port environment, including its geographical setting, spatial distribution of economic activities and key port assets, as well as relevant bathymetric, and topographic features influencing tsunami propagation. This initial step provides the spatial and functional context required to identify key port assets and activities, serving as the basis for subsequent hazard, exposure, and vulnerability assessments.

Building on the port characterisation stage, the subsequent analytical component of the framework involves **tsunami hazard assessment**. This component focuses on the identification of potential tsunami scenarios and characterisation of tsunami-generating sources relevant to the study area, together with the numerical simulation of tsunami generation, propagation, and inundation processes required to characterise the hazard within the port environment.

https://doi.org/10.5194/egusphere-2026-4720
Preprint. Discussion started: 14 August 2026
© Author(s) 2026. CC BY 4.0 License.

The **exposure assessment** focuses on identifying and quantifying the elements within the inundation area for each hazard scenario, including port infrastructure (e.g., warehouses, buildings, and access ramps), commercial assets (e.g., containers, Ro-Ro, and storage tanks) and population (including port workers and passenger terminal users).

The **vulnerability assessment** component examines the susceptibility of exposed elements within the port to tsunami impact, by defining damage levels for the asset types considered in the analysis. Accordingly, the **risk assessment** evaluates the potential consequences arising from tsunami impact on exposed port area assets and population.

Within this framework, risk is assessed in terms of direct physical damage to exposed assets caused by tsunami-induced inundation and hydrodynamic loads. The analysis therefore focuses on impacts that may compromise the structural integrity or physical functionality of critical port assets, including cargo-handling equipment, containers, vehicles, storage tanks, and areas with human presence. Figure 1 illustrates the conceptual scheme of the proposed methodological framework, which is described in the following sections.

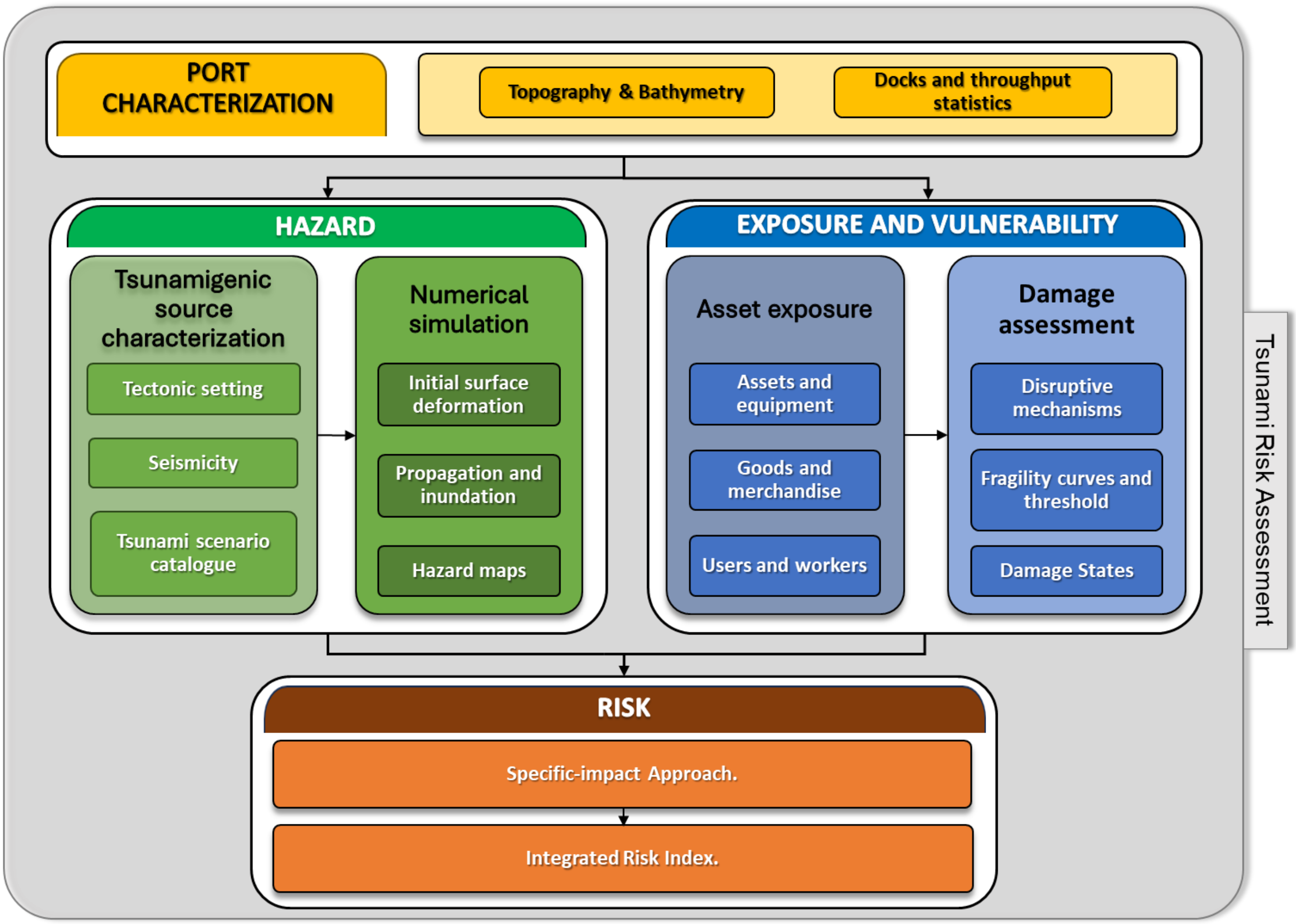

Figure 1. Conceptual scheme of the methodological framework for tsunami risk assessment in port's landside operational area.

https://doi.org/10.5194/egusphere-2026-4720
Preprint. Discussion started: 14 August 2026
© Author(s) 2026. CC BY 4.0 License.

2.1. Port description and characterization

The objective of this section is to characterise the spatial, physical, and functional features of the port that condition tsunami propagation and asset exposure. This characterisation provides the contextual information required to support the subsequent assessment of hazard, exposure, and vulnerability within the proposed framework, and is conducted at two complementary spatial scales: regional and local.

At the regional level, the main geomorphological characteristics that influence the propagation of the tsunami to the port area must be identified. These elements encompass the characteristics of the continental shelf, the presence of extensive submarine canyons, islands, the configuration of the coastline, and the location of the port facility within bays or estuaries (harbor). Additionally, tidal information must be considered in areas subject to mesotidal or macrotidal influences. The aforementioned factors can alter tsunami propagation, potentially leading to wave amplification and resonance effects within the port environment (Roig-Munar et al., 2017; Vela et al., 2014; Wilson et al., 2017). Consequently, an accurate characterisation of these regional-scale features is essential for the definition of tsunami hazard scenarios.

At the local scale, a detailed characterization of the port configuration is required to support the assessment of asset exposure and subsequent impact. This characterization involves the acquisition of three main types of information: (i) high-resolution topographic and bathymetric data, (ii) detailed plans of the port's landside operational areas, and (iii) operational statistics describing port activities. Port discretization is essential to effectively analyse the docks, including their dimensions, primary applications, and the spatial distribution of existing port infrastructure.

To facilitate local-scale analysis, port terminals can be broadly classified into five main groups according to their primary activity: commercial, industrial, fishing, tourism, and military ports (Puertos Del Estado, 2012). However, ports rarely correspond to a single functional category. In practice, most ports perform, to varying degrees, several of the functions associated with these categories (Puertos Del Estado, 2009). This functional classification provides an initial indication of the types of assets and activities likely to be present within each terminal and, consequently, of the elements potentially exposed to tsunami hazards.

From a physical perspective, a port terminal can be subdivided into three primary areas (see Figure 2): the water area, the berthing area, and the landside area. The latter constitutes the main focus of the proposed risk assessment framework, as it contains the fixed and mobile assets that support port operations and are directly exposed to tsunami-induced inundation and hydrodynamic forces.

https://doi.org/10.5194/egusphere-2026-4720
Preprint. Discussion started: 14 August 2026
© Author(s) 2026. CC BY 4.0 License.

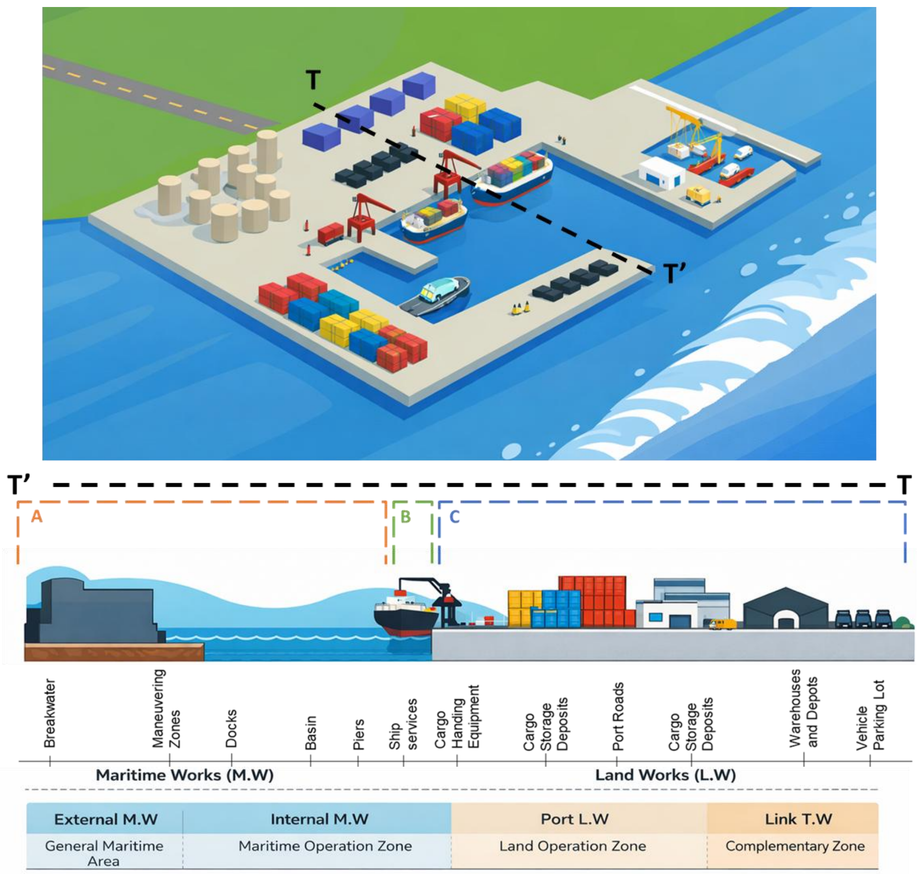

Figure 2. Plan view (top figure) and profile (bottom figure) illustrating a port terminal. Through the cross-section TT', the three different areas of a port terminal can be seen: A. Water Area. B. Berthing Area, and C. Landside Area.

This port discretization aims to identify the minimum set of spatial characteristics required to achieve a preliminary understanding of the areas that may influence, to varying degrees, tsunami wave propagation within the port, as well as the operational zones potentially exposed to impact, the associated economic activities, and the port assets involved. This level of discretization is essential to support a consistent assessment of exposure and subsequent vulnerability at dock and terminal scales.

Accordingly, the objective of this stage is to compile all relevant characteristics identified at both regional and local scales, including high-resolution topographic and bathymetric data and detailed port planimetry, incorporating dock geometry and logistical activities. The use of Geographic Information System (GIS) tools and formats is strongly recommended to ensure a spatially explicit and integrated representation of port assets, providing the necessary basis for the subsequent exposure and vulnerability assessments within the proposed risk assessment framework.

The characterization should incorporate information on the main port assets, their spatial distribution, and the operational activities associated with them. Table 1 presents an example of the attributes employed to describe these elements within the

https://doi.org/10.5194/egusphere-2026-4720
Preprint. Discussion started: 14 August 2026
© Author(s) 2026. CC BY 4.0 License.

proposed framework and subsequently applied in the case study. In addition to detailed port planimetry, the database should incorporate information on terminal logistics activities and asset occupancy. Relevant indicators may include vehicle-storage occupancy rates, container stacking capacity and utilization, the proportion of empty containers, and the annual number of passengers and workers using the port.

Table 1. Template for port characterization; this includes the basic information about the port required to conduct a risk assessment of the port's landside operational area.

Asset	Item	Attributes
Containers	Spatially referenced maps of the storage areas	• Average annual container volume, in TEUs (*Twenty-foot Equivalent Units*). • Max. number of stacks for each lot. • Type (empty/refrigerated/high cube...).
Ro-Ro and parking lots	Spatially referenced maps of the storage areas	• Parking lot locations. • Ro-Ro transport locations.
Building & Warehouses	Spatially referenced maps of the storage buildings	• Construction material. • Dimensions. • Usage.
Pedestrians	Spatially referenced maps of the storage areas	• Pedestrian walkways. • Average passenger volume. • Passenger waiting and rest areas. • Security and customs checkpoints.
Storage Tanks	Spatially referenced maps of the storage areas	• Dimensions (Diameter, height). • Storage material (density).
Cargo Handling equipment	Spatially referenced maps of the storage areas	• Type (mobile cranes, specialized gantry cranes). • Application (material handled). • Dimensions. • Weight.
Roadways	Spatially referenced maps of the roadways	• Route Maps.

3. Tsunami Hazard Assessment

The objective of this section is to define the approach for tsunami hazard assessment within the proposed risk framework, from the stochastic characterization of the seismic sources to the accurate modelling of local tsunami inundation and the derivation of hazard intensity measures. This step sets out the minimum methodological requirements to understand the hydrodynamic loads that may affect port facilities, with particular emphasis on the landside operational area and structures located along docks and wharves. The proposed hazard assessment framework is independent of the hazard quantification approach and can be implemented using either scenario-based or probabilistic methods.

https://doi.org/10.5194/egusphere-2026-4720
Preprint. Discussion started: 14 August 2026
© Author(s) 2026. CC BY 4.0 License.

In a scenario-based implementation, tsunami hazard may be characterised through the evaluation of the so-called credible worst-case tsunami scenarios, as commonly adopted in deterministic tsunami studies (Álvarez-Gómez et al., 2013; Chua et al., 2024; Popovich et al., 2021) that could affect the port's landside operational area.

Seismotectonic scenario selection should consider the interaction between tsunami source characteristics and the natural oscillation modes of the continental shelf, adjacent bays, and port basins (Aranguiz et al., 2019; Dong et al., 2020; Masina et al., 2020; Yalciner and Pelinovsky, 2007). Under certain conditions, the coincidence between tsunami wave periods and the natural periods of these coastal systems may significantly amplify the hydrodynamic response and tsunami run-up within port environments. Therefore, a resonance analysis at both regional and local scales is recommended to identify the dominant oscillation modes and resonant periods of the continental shelf, bays, and port domain (Aranguiz et al., 2019; Roeber et al., 2010; Yalciner and Pelinovsky, 2007; Yamazaki and Cheung, 2011). For this purpose, numerical models capable of solving the Mild-Slope Equation (MSE) may be employed (Dong et al., 2020; Ma et al., 2020).

In addition to the resonance analysis, it is recommended to characterize the dominant wave periods associated with tsunamigenic earthquakes across a range of moment magnitudes (Mw) for the considered sources (Aniel-Quiroga et al., 2018). This analysis supports the definition of a representative set of tsunami scenarios for subsequent numerical simulation and inundation assessment.

The combined application of these approaches provides a robust framework for the identification of credible worst-case inundation scenarios within port landside operational area, supporting tsunami hazard characterization.

In a probabilistic implementation of the hazard assessment framework, tsunami hazard can be quantified using probabilistic tsunami hazard assessment (PTHA) which estimates the probability of exceeding a given hazard intensity at a specific location over a defined time interval (Gibbons et al., 2020). This approach relies on stochastic models to simulate a comprehensive array of potential tsunami scenarios, their associated occurrence probabilities, and the resulting hazard at a coastal site (Wannous and Velasquez, 2017). Within this framework, epistemic and aleatory uncertainties are incorporated to derive hazard curves describing the annual exceedance rates of selected tsunami intensity measures (TIMs), such as inundation depth, flow velocity, or momentum flux (Basili et al., 2021; Behrens et al., 2021).

The procedure involves two essential steps: the characterization of tsunami-generating sources (selection of seismic sources relevant to the analysis and creation of a scenario catalog) and the numerical tsunami simulations (collection of topobathymetric baseline data, construction of nested grids, and generation of hazard maps for the necessary hydrodynamic variables).

3.1. Characterization of tsunami-generating sources

Characterization of tsunami-generating sources constitutes a fundamental input for the tsunami hazard assessment framework, providing the parameters required for numerical modelling of tsunami generation and subsequent propagation towards port environments. In general, the characterization of tsunami-generating sources consists of:

https://doi.org/10.5194/egusphere-2026-4720
Preprint. Discussion started: 14 August 2026
© Author(s) 2026. CC BY 4.0 License.

- A seismotectonic study based on historical events to understand the characteristics of tsunami-generating earthquakes that could affect the study area.
- An analysis of the tectonic setting. The process encompasses the establishment of global-regional source domains, followed by their discretization into unit sources or patches. This observation suggests the possibility of multiple seismic source scenarios (characterizing the main active faults).
- A seismicity study for each source, to characterize the ruptures of the earthquakes considered. The approach entails the generation of a synthetic catalogue of seismic events, employing a framework that incorporates random sampling of magnitude, mechanism, and slip distribution. The objective is to accurately represent the probability of occurrence and natural variability.

Regional hazard models such as NEAMTHM18 (Basili et al., 2021) can be employed, supported by disaggregation analyses to identify scenarios contributing most significantly to the hazard in port-prone areas (Gibbons et al., 2020).

The resulting source parameters provide the necessary inputs for numerical tsunami generation models, in which coseismic seafloor deformation associated with earthquake rupture is computed using the Okada formulation (Okada, 1985).

3.2. Tsunami generation and propagation

Once defined, the selected tsunami scenarios should be simulated numerically to reproduce tsunami generation, propagation, and inundation within the port environment. This process is based on the computation of coseismic seabed deformation and the subsequent numerical modelling of wave propagation from regional to local scales.

To this end bathymetry and topography databases with a consistent vertical reference are required, to accurately represent the coastal and port domains. Topographic and bathymetric datasets are integrated and nested computational grids are constructed, typically ranging from regional resolutions to local resolutions on the order of a few metres. Multiple data sources are commonly combined, including bathymetric surveys, detailed nautical charts, including high-resolution digital elevation models.

Numerical tsunami simulation in port environments commonly relies on nested mesh systems to ensure that the various physical scales involved are resolved in a consistent manner. The computational domain is usually divided into three distinct domains: (i) the open ocean, where linear propagation processes predominate; (ii) the coastal zone, where bathymetric transitions require higher spatial resolution, due to variations in coastline geometry and bathymetry that may induce resonant phenomena; and (iii) the port domain, characterized by reflection processes, strong nonlinear behaviour such as resonances and spatially amplified patterns (Aranguiz et al., 2019; Gao et al., 2019; Vela et al., 2014), and potential dispersion patterns.

The selection of the hydrodynamic model must be based on the dominant physical processes in each domain. The hydrodynamic challenge in ports requires the selection of numerical models that incorporate (at least) the properties of nonlinearity in intermediate and shallow waters (Watts et al., 2003). The literature identifies three broad classes of hydrodynamic models applied to tsunamis, organized based on the complexity of the physics they solve and their numerical robustness (Lynett et al., 2017; Marras and Mandli, 2020): (i) Nonlinear Shallow Water Equations (NLSWE) models, which

https://doi.org/10.5194/egusphere-2026-4720
Preprint. Discussion started: 14 August 2026
© Author(s) 2026. CC BY 4.0 License.

solve vertically averaged equations under the hydrostatic approximation (without dispersive terms), they achieve second-order accuracy and are notable for their robustness in run-up areas and wetting–drying fronts (Berger et al., 2011; Macías et al., 2020b, a; Wang, 2009); (ii) Boussinesq-type models, which incorporate dispersive effects using third- or fourth-order dispersive terms and more accurately represent wave transformation in intermediate waters, although they require more complex treatment of friction, breaking, and dispersion (Choi et al., 2022; Kim et al., 2009; Shi et al., 2012; Yuan et al., 2020); and (iii) non-hydrostatic Navier–Stokes models (e.g., RANS type), capable of resolving turbulence, air–water processes, and three-dimensional dynamics (Horrillo et al., 2013; Zhang et al., 2016); these are generally limited for very local domains, due to their high computational demand.

Following the execution of a specified number of stochastic simulations, the tsunami intensity measures such as maximum inundation depth, maximum flow velocity or maximum momentum flux are extracted at each point of the highest resolution grid. These results are subsequently combined to generate hazard maps using either deterministic or probabilistic approaches. In a deterministic approach, the results are typically conveyed through the implementation of aggregated maps (Álvarez-Gómez et al., 2013), in which the maximum value of the simulated variables is selected for each point. This approach offers a comprehensive representation, encompassing all the information from the considered scenarios, which collectively highlight the most unfavorable hazard conditions. In probabilistic implementations, hazard curves are used to derive expected intensities associated with specific probabilities of exceedance or average return periods (Basili et al., 2021), from which corresponding hazard maps can be generated.

4. Assessment of the exposure and vulnerability of the main elements in the Port's landside operational area

In port environments, **exposure** encompasses all onshore assets, goods, and human elements that could be affected by a tsunami, whereas vulnerability represents the susceptibility of those exposed elements to damage given a certain tsunami intensity (UNDRR, 2025). This issue assumes particular significance due to the high concentration of critical assets, their typological diversity, and the strong operational interdependence between them. In contrast to conventional urban environments, ports exhibit a high degree of heterogeneity in terms of spatial and functional behaviours, requiring a differentiated approach to exposure assessment in order to ensure reliable potential damage estimates.

Following the characterisation of exposure, **vulnerability is defined** as the susceptibility of an element to suffer damage under the action of a tsunami event, being intrinsically linked to its physical characteristics, such as geometric configuration, construction materials, and level of maintenance (Heintz and Robertson, 2008; UNDRR, 2025). The proper characterization of vulnerability constitutes a fundamental step in risk quantification, as it allows the estimation of the considered asset damage states as a function of the hydrodynamic variables associated with the event.

It is important to note that the Tsunami Intensity Measures (TIM) used to assess the effects on port assets are recommended to correspond to the maximum values reached during the simulated event; These may include maximum inundation depth, the maximum flow velocity (averaged vertically), or the maximum momentum flux ($(hU^2)_{max}$). Because a given asset may extend

https://doi.org/10.5194/egusphere-2026-4720
Preprint. Discussion started: 14 August 2026
© Author(s) 2026. CC BY 4.0 License.

over multiple nodes of the computational grid, it is recommended that the representative TIM adopted for the vulnerability assessment should correspond to the maximum value identified within the spatial extent of that asset.

4.1. Exposure Assessment of the port's main assets and goods.

Port environments are characterised by a high degree of spatial and operational heterogeneity, encompassing assets with distinct physical characteristics, functions, and temporal occupancy patterns. To represent this heterogeneity within the proposed risk assessment framework, two complementary approaches may be considered: static exposure and dynamic exposure. **Static exposure** refers to assets whose location and attributes are assumed to remain constant during the considered scenario, such as buildings, fixed port infrastructure, and designated pedestrian areas. Conversely, **dynamic exposure** accounts for port assets whose quantity, occupancy, operational status, or physical characteristics may vary over time, directly influencing damage estimates.

The dynamic exposure approach considers assets whose characteristics or occupancy conditions may vary over time. Relevant examples include the fill level of liquid bulk storage tanks (Cruz et al., 2011; Goyo, 2008; Hatayama, 2017; Naito et al., 2013; Vitale et al., 2024), the occupancy of Ro-Ro storage areas, and the stacking and weight configurations of container storage yards (Elkafas et al., 2019; Kumagai, 2013; Lee et al., 2024; Tran et al., 2019). These assets are characterised by temporal variability in their quantity, occupancy, operational condition, physical characteristics, or spatial distribution. Appropriate metrics and statistical parameters can therefore be used to represent this variability and support a more realistic estimation of exposure and vulnerability under a given hazard scenario.

For storage tanks, exposure characterisation may be addressed through the definition of discrete fill states representing different operational conditions. Similarly, the exposure of general and containerized cargo may be characterized using discrete probability distributions, such as uniform, Bernoulli, or binomial distributions. These distributions can be used to represent variables including storage occupancy, the proportion of empty and loaded containers, and the number of containers stacked within designated storage areas.

For these variables, probability distributions may be truncated to ensure that samples remain within physically and operationally feasible ranges. A Monte Carlo simulation approach may then be used to quantify dynamic exposure by accounting for the variability of tank fill levels, storage occupancy, and container stacking configurations. The resulting exposure estimates can subsequently be incorporated into dock-level risk aggregation. The applicability and robustness of the exposure assessment depends on the availability and quality of the information related to port throughput statistics.

Overall, the combined use of static and dynamic exposure approaches provides a more realistic representation of the operational and structural complexity of ports, supporting improved damage estimation and subsequent risk aggregation analyses at the dock level.

Based on the asset characterization conducted during the exposure assessment, an Exposure Index (EI^{dock}) can be calculated for each dock. This index provides a quantitative measure of the relative concentration of assets at dock scale, facilitating the

https://doi.org/10.5194/egusphere-2026-4720
Preprint. Discussion started: 14 August 2026
© Author(s) 2026. CC BY 4.0 License.

identification of areas with higher or lower exposure levels. The index is calculated from the relative proportion of each asset type present at a given dock with respect to the total inventory of that asset type within the port, as expressed in Eq. (1):

$$\boldsymbol{EI^{dock}} = \sum \frac{Asset_i^{dock}}{Asset_i^{port}} \quad (1)$$

Where $Asset_i^{dock}$ is the total number of units of asset type i present at the dock, and $Asset_i^{port}$ is the total number of units of the same type within the port.

After calculating the EI^{dock}, the resulting relative values should be categorised into nominal exposure levels to support interpretation and comparison between port sections. This can be achieved using objective classification methods, such as k-means clustering, Jenks natural breaks, or other data-driven discretization techniques, which allow the continuous index values to be grouped into relative classes, such as low, medium, and high exposure.

4.2. Tsunami Vulnerability Assessment of port assets

The main objective of this step is to establish a consistent methodological basis for assessing direct physical damage to the main assets associated with the supply chain in the port's landside operational area. To this end, an extensive review of the literature addressing tsunami impacts on port-related assets has been conducted, together with an analysis between tsunami hydrodynamic variables, and the damage observed in historical events.

In this context, experimental, empirical and analytical studies play a key role in quantifying the loads exerted by tsunamis and in deriving damage–intensity relationships (Chua et al., 2021; Ferrotto and Cavaleri, 2021; Koshimura et al., 2009; Macabuag et al., 2018; Shoji and Moriyama, 2007). Fragility functions provide a statistical representation of this relationship, describing the probability of an asset exceeding a given damage state as a function of a TIM (Charvet et al., 2017; Song et al., 2017).

Within the context of port operations, it is particularly advantageous to translate this information into a semi-quantitative approach by employing damage thresholds (Argyroudis et al., 2016; González-Riancho et al., 2014; Nagi et al., 2021; Rafliana et al., 2022; Williams et al., 2019). Compared with a continuous representation of failure probability, damage thresholds synthesise the information contained in fragility functions into discrete impact-levels, thereby facilitating their integration into decision-making processes.

The assessment of tsunami-induced damage requires a clear and consistent classification of the different damage states (DS) (Charvet et al., 2017; Kazama and Noda, 2012). This classification scheme provides a set of mutually exclusive and sequential damage states applicable to the different asset types considered within the landside operational area.

This threshold-based formulation allows damage states to be directly assigned by combining the maximum tsunami intensity affecting a given asset with a set of predefined damage thresholds. These damage states can subsequently be integrated with exposure indicators to support aggregated dock-level risk calculations within the proposed framework. The Damage State Function (DS) represents progressive increasing levels of damage severity, as shown in Figure 3:

https://doi.org/10.5194/egusphere-2026-4720
Preprint. Discussion started: 14 August 2026
© Author(s) 2026. CC BY 4.0 License.

$$DS = f(x) = \begin{cases} DS_0, & 0 < IM_{max} \leq \theta_1 \\ DS_1, & \theta_1 < IM_{max} \leq \theta_2 \\ & \vdots \\ DS_{k-1}, & \theta_{k-1} < IM_{max} \leq \theta_K \\ DS_k, & IM_{max} > \theta_K \end{cases} \rightarrow$$

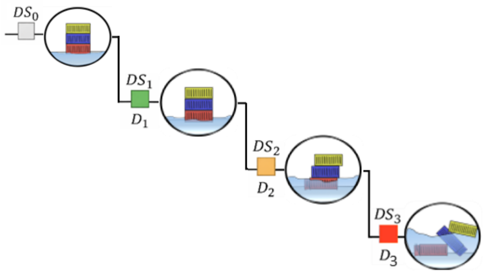

Figure 3. Damage State Function (DS). The left-hand side of the figure provides the definition of thresholds for a given asset, while the right-hand side shows an illustrative representation of the various damage states.

The proposed fragility methodology, based on the concept of thresholds, has the potential to enhance risk communication and facilitate its integration into tsunami planning and response strategies (Argyroudis et al., 2016; Nagi et al., 2021).

The vulnerability assessment developed in this study focuses on the main assets of the port supply chain that have historically been affected by tsunami impacts. These include cargo handling equipment, storage facilities, (e.g., office buildings and warehouses), storage tanks, cargo units (containerized, Lo-Lo or Ro-Ro) and people, since historically, these are the assets that have been most affected (CGS, 2025; Chua et al., 2021; Cruz et al., 2011; Imai et al., 2019; Oda et al., 2007; Percher et al., 2013; Percher, 2014; Suppasri et al., 2022; Takahashi et al., 2010; Tran et al., 2019; Williams et al., 2019).

4.2.1. Cargo handling equipment

According to the technical criteria established by (Puertos Del Estado, 2012), cargo-handling cranes are strategic assets that enable the efficient transfer of goods between ships and land, directly influencing the terminal productivity and competitiveness.

Historical tsunami events have repeatedly demonstrated the vulnerability of port cargo-handling equipment. For example, the 1946 and 1960 tsunamis caused recurrent damage to the port facilities in Hilo, Hawaii, following the events in the Aleutian Islands and Chile, respectively (Lynham et al., 2017). The 1960 Valdivia mega-earthquake and tsunami also affected several ports in Chile and the Pacific region, including the Port of Corral where cargo-handling equipment and aging steel cranes suffered significant damage (Lomnitz, 2004). Similarly, the 2004 Indian Ocean tsunami caused extensive damage to port cranes (Synolakis and Kong, 2006), while the 2011 Tohoku tsunami affected cargo-handling equipment in several Japanese ports, including Sendai-Shiogama and Soma.

Observed damage to port cranes is primarily attributed to the direct impact of tsunami waves, undermining and loss of structural support, and collision with drifting vessels or containers (Percher, 2014; Takahashi et al., 2014). In recent years, studying structural vulnerability to tsunamis has become increasingly important in coastal and port engineering. However, most studies have focused on civil infrastructure, such as buildings and bridges, while fewer have examined cargo handling equipment specifically.

https://doi.org/10.5194/egusphere-2026-4720
Preprint. Discussion started: 14 August 2026
© Author(s) 2026. CC BY 4.0 License.

Among the studies that quantitatively assess the vulnerability of cargo-handling equipment to tsunamis is the work of Koshimura et al., (2009). They performed numerical simulations of the 2004 tsunami in several Southeast Asian ports and estimated areas of high structural vulnerability. Although cranes were not the main focus of their work, proxies were used for port metal structures.

Conversely, the study by Chua et al. (2021) represents one of the most comprehensive empirical assessments of the vulnerability of cargo-handling equipment in port environments, including cranes and conveyor systems. The authors analyzed hundreds of cargo-handling equipment units affected by tsunami events through detailed photographic interpretation and post-disaster surveys. The observed damage was correlated with the Tsunami Intensity Measure (TIM) inundation depth (*h*), allowing for the development of empirical fragility curves for several identified damage states (DS). These fragility curves, shown in Figure 4, express the conditional probability of exceeding a given damage state as a function of inundation depth.

In the present study, the thresholds defining the damage states were derived from the fragility relationships proposed by Chua et al. (2021). Specifically, the inundation depth associated with a 50 % exceedance probability was adopted as a representative threshold for each damage state. This value corresponds to the median of the fitted fragility relationship and provides a consistent operational criterion for translating continuous fragility information into discrete damage-state thresholds. Based on these thresholds, the damage-state function presented in Table 2 has been proposed in this work.

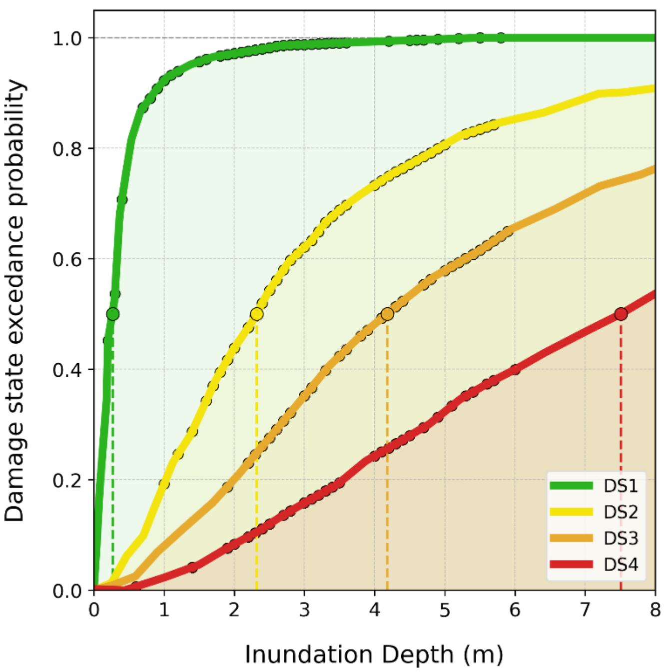

Figure 4. Representation of the selection of damage thresholds for the TIM inundation depth. The fragility curves for assets related to cargo handling are shown. Based on the results taken from Chua et al. (2021). The green, yellow, orange, and red lines represent damage states DS1, DS2, DS3, and DS4, respectively. The scattered points behind the curves shown in the figures correspond to data surveyed at various ports in Japan following the 2011 Tohoku tsunami.

https://doi.org/10.5194/egusphere-2026-4720
Preprint. Discussion started: 14 August 2026
© Author(s) 2026. CC BY 4.0 License.

Table 2. Description and definition of a proposed damage state function for cargo handling equipment.

DS	TIM Max. Inundation depth $\boldsymbol{h}\ (\boldsymbol{m})$	Description	
Very Low	$h \leq 0.5$	There is no visible damage or other effects.	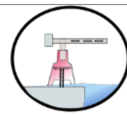
Low	$0.5 < h \leq 2.0$	It gets wet due to flooding, but there is no damage.	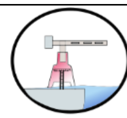
Medium	$2.0 < h \leq 4.0$	There is some damage to the infrastructure, but the foundation or base remains intact.	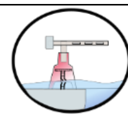
High	$4.0 < h \leq 7.0$	The foundation or base of the infrastructure has bent or warped. It may collapse.	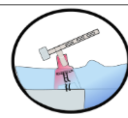
Very high	$h > 7.0$	The infrastructure has overturned or slid from its original position.	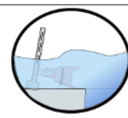

4.2.2. Warehouses and buildings

This asset category includes storage warehouses, customs buildings, garages, commercial buildings, and other facilities that support the reception and storage of goods within port operations. Historical evidence from past tsunami events provides a basis for analysing the relationship between hydrodynamic variables and structural resistance (Lekkas et al., 2013; Rehman and Cho, 2016; Tarbotton et al., 2015).

Several factors contribute to the level of damage suffered by port buildings during a tsunami, including the characteristics of the building itself and the hydrodynamic characteristics of the tsunami. Empirical studies have established relationships between inundation depth and various levels of damage for different types of buildings, providing a basis for impact assessment (Chua et al., 2021; Suppasri et al., 2019).

Charvet et al., (2017) provides a compilation of studies analyzing building vulnerability based on post-tsunami events, with the aim of outlining the limitations and significant advances in this field. The information presented in this study was essential

https://doi.org/10.5194/egusphere-2026-4720
Preprint. Discussion started: 14 August 2026
© Author(s) 2026. CC BY 4.0 License.

for defining building damage states (DS). Furthermore, post-tsunami data collected from reinforced concrete buildings (the most common building type found in port environments) affected by the 2011 Tohoku tsunami and the 2004 Indonesian tsunami have enable the estimation of threshold values associated with each damage state for more than 250 thousand buildings surveyed through field inspection and satellite imagery (Suppasri et al., 2013, 2015). These results have made it possible to identify TIM ranges within which damage states are most likely to occur. For example, (Valencia et al., (2011) found that minor damage would occur at inundation depth less than 2.5 m, moderate damage at depths greater than 3 m, and total destruction at depths greater than 7 m, findings that are consistent with those reported by Dias and Edirisooriya (2019) and Reese et al. (2011).

Similarly to cargo-handling equipment, Chua et al. (2021) investigated the vulnerability of warehouse facilities exposed to tsunami inundation within port environments. The fragility curves proposed by Chua et al. (2021), shown in Figure 5, were used in the present study to define the damage thresholds for warehouse facilities. The inundation depth associated with a 50% probability of exceedance, $P(DS > ds|h) = 0.5$, was selected as the representative reference threshold for each damage state. Table 3 describes a proposed approach for assessing the direct impacts on this asset category. It presents the damage states (DS), a description of the expected damage, and thresholds based on the maximum inundation depth ($\boldsymbol{h}$) at each damage level.

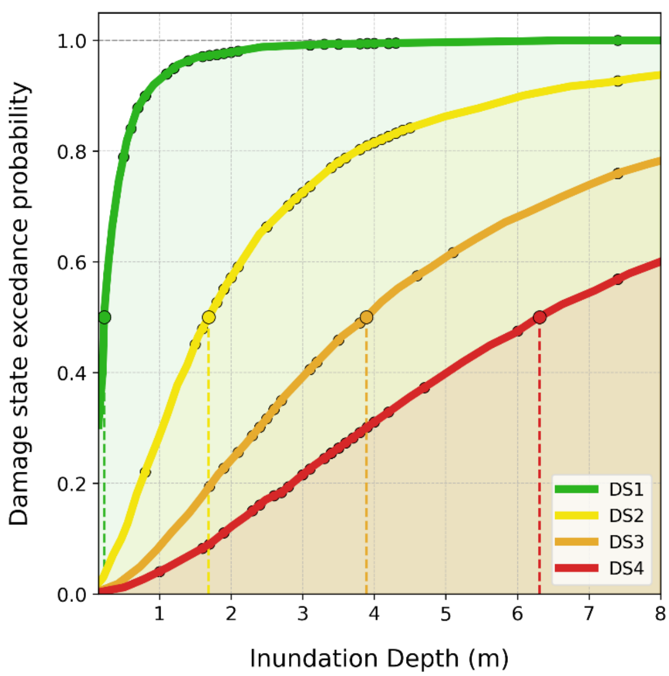

Figure 5. Representation of the selection of damage thresholds for the TIM inundation depth. The fragility curves for assets related to warehouse are shown. Based on the results taken from Chua et al. (2021). The green, yellow, orange, and red lines represent damage states DS1, DS2, DS3, and DS4, respectively. The scattered points behind the curves shown in the figures correspond to data surveyed at various ports in Japan following the 2011 Tohoku tsunami.

© Author(s) 2026. CC BY 4.0 License.

Table 3. Description and definition of a proposed damage state function for port buildings and warehouses.

DS	TIM Max. Inundation depth $\boldsymbol{h}$ $(\boldsymbol{m})$	Description	
Very Low	$h \leq 0.5$	The structure has been exposed to flooding, but there is very low probability to have observable damage	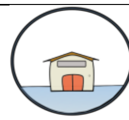
Low	$0.5 < h \leq 1.5$	The structure has been exposed to flooding, but there has been no observable damage.	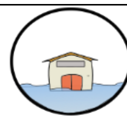
Medium	$1.5 < h \leq 3.0$	Some damage to the infrastructure, while the foundations or base remain intact.	
High	$3.0 < h \leq 6.0$	The foundation or base of the infrastructure has bent or warped. It may have collapsed.	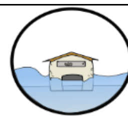
Very high	$h > 6.0$	The infrastructure has overturned or slipped from its original position.	

4.2.3. Storage tanks

Port infrastructure dedicated to the storage of liquid bulk cargo constitutes a critical backbone for key industries such as the energy, chemical, food, and pharmaceutical sectors (UAB, 2025). Historical tsunami events provide a crucial empirical basis for understanding failure mechanisms and the consequences of tsunami impacts on liquid bulk storage tanks. These case studies enable the identification of damage patterns and the extraction of valuable lessons to inform mitigation design and planning. The 2004 Indian Ocean tsunami caused extensive damage to oil storage tanks, particularly in the province of Aceh (Goyo, 2008). A key observation was the high vulnerability of tanks containing little stored material, as they were easily lifted and moved (Tang et al., 2006). The 2011 Tohoku tsunami represented a critical case study for tsunami impacts, with damage recorded to more than 400 storage tanks, of which 157 were displaced from their original positions (Hatayama, 2015). According to post-event survey data, the observed failure modes include (i) crushing of tanks due to inward hydrostatic forces; (ii) failures in fastening systems due to high buoyancy forces; and (iii) slippage failures caused by tsunami-induced hydrodynamic forces (Heintz and Robertson, 2008; Naito et al., 2013).

https://doi.org/10.5194/egusphere-2026-4720
Preprint. Discussion started: 14 August 2026
© Author(s) 2026. CC BY 4.0 License.

Post-tsunami studies have shown that, despite systematic failure modes, threshold values of TIM values, such as maximum inundation depth and maximum flow velocity, associated with a specific damage state do not necessarily remain constant, as tank dimensions and fill levels can significantly influence their vulnerability (Hatayama, 2015; Naito et al., 2013; Tang et al., 2006). Consequently, the findings of this study are not directly transferable to other ports (Gao et al., 2022; Yoshida, 2018).

A variety of studies have proposed functions to estimate damage based on empirical analyses (Cruz et al., 2011; Hatayama, 2015; Naito et al., 2013; Vitale et al., 2024; Williams et al., 2019). In general, global structure failure is the result of at least one governing failure mode (Heintz and Robertson, 2008; Naito et al., 2013). It is therefore proposed that the fragility of this asset be assessed through an analysis of forces.

The stability of above-ground cylindrical storage tanks subjected to tsunami inundation was assessed considering two primary failure mechanisms: flotation due to buoyancy forces and sliding caused by the combined action of hydrostatic and hydrodynamic loads (see Figure 6). The storage tank is represented as a vertical cylindrical steel structure characterized by its radius (R) and height (H_{tank}). Its structural mass was estimated from the shell and bottom volumes, while the stored-liquid mass was computed from the internal volume, crude-oil density, and filling ratio. For sliding, the procedure compared the horizontal tsunami-induced loading with the frictional resistance at the tank–foundation interface. The driving force was represented by the sum of hydrostatic and hydrodynamic drag components. The hydrostatic component F_{hs} is approximated as (Eq. 2):

$$F_{hs} = \rho \cdot g \cdot R \cdot {h_{sub}}^2 \tag{2}$$

Where g is the gravity, h_{sub} is the maximum inundation depth. Although it is generally less than dynamic forces, it becomes significant when the inundation caused by the tsunami rises rapidly (Nouri et al., 2007). The drag force F_d, is calculated as (Eq. 3):

$$F_d = \rho \cdot C_d \cdot R \cdot h_{sub} \cdot U^2 \tag{3}$$

The drag coefficient, C_d is defined as 1.2, according to Yamamoto et al. (2021), ρ is the density of seawater and U represents the depth-averaged maximum flow velocity (for maximum F_d). Likewise, the available resisting force F_{res} defined by Eq. (4).

$$F_{res} = \mu \cdot m \cdot g \tag{4}$$

The mass of the stored crude oil is calculated as (Eq. 5):

$$\boldsymbol{m = \rho_{oil} \cdot \pi \cdot R^2 \cdot H_{tank} \cdot f_{\%}}. \tag{5}$$

Where $f_{\%}$ denotes the filling ratio. The sliding failure condition is therefore defined as (Eq. 6):

$$F_{hs} + F_d \geq F_{res} \tag{6}$$

The velocity-dependent sliding solutions are subsequently approximated using a power-law relationship of the form. $hU^2 = k$. This allows the sliding maximum threshold k to be expressed directly in terms of flow depth and velocity. For a prescribed flow velocity, the critical inundation depth is obtained numerically by solving the equilibrium equation using a bisection algorithm. The numerical solutions indicate that the sliding threshold can be represented by a hyperbolic relationship between

https://doi.org/10.5194/egusphere-2026-4720
Preprint. Discussion started: 14 August 2026
© Author(s) 2026. CC BY 4.0 License.

inundation depth and squared velocity. The velocity-dependent sliding solutions are subsequently approximated using a power-law relationship of the form (Eq. 7):

$$h * U^2 = k_{slide} \quad (7)$$

Where k_{slide} is a fitting critic parameter that depends on the tank geometry and filling condition. The coefficient k_{slide} is obtained through ordinary least-squares regression using the computed instability points. This formulation allows the sliding threshold to be expressed directly in terms of momentum flux can be readily incorporated into tsunami risk models based on momentum flux.

For flotation, the tsunami-induced buoyancy force was calculated using Archimedes' principle, assuming that the displaced volume corresponds to the submerged cylindrical volume. The critical flotation depth was defined as the inundation depth at which the buoyancy force equals the total downward weight of the tank system. This maximum threshold depends on tank geometry, material properties, and filling condition. The resultant vertical force (Eq.8), represents the upward force exerted by the displaced water on the storage tank. This phenomenon reduces the net weight of the structure and may lead to flotation (Yeh et al., 2014).

$$F_B - W_{Tf} \geq 0 \quad (8)$$

The quantity W_{Tf} signifies the weight of the liquid bulk cargo plus the tare weight of the storage tank, and the buoyancy force F_B is defined as in (Eq. 9).

$$F_B = g * \rho * Vol_{sub} \quad (9)$$

Where Vol_{sub} is the submerged volume of the object. This implies that vertical stability is governed by F_B, and the asset will begin to float when F_B is greater than W_{Tf}. Substituting the above expressions yields the critical flotation depth h_{flot} (Eq. 10):

$$h_{flot} = \frac{W_{Tf}}{\rho \cdot g \cdot \pi \cdot R^2} \quad (10)$$

This maximum threshold depends exclusively on tank geometry and filling condition.

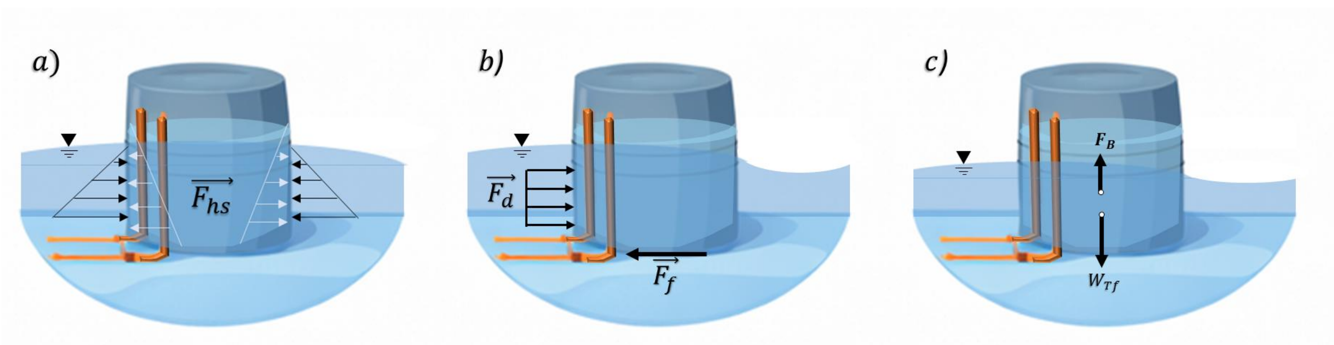

Figure 6: Diagram of forces present under the action of a) hydrostatic forces, b) Hydrodynamic forces, and c) Buoyancy forces acting on a liquid bulk storage tank due to the impact of a flooding caused by a tsunami.

https://doi.org/10.5194/egusphere-2026-4720
Preprint. Discussion started: 14 August 2026
© Author(s) 2026. CC BY 4.0 License.

Finally, the ultimate instability thresholds obtained for flotation and sliding were translated into three damage states by scaling the critical values: DS1 for values below 30 % of the maximum threshold, DS2 for values between 30 % and 100 %, and DS3 for values exceeding the maximum threshold. Thus, the method provides, for each filling condition, a critical flotation depth, a critical sliding coefficient, and corresponding damage thresholds based on maximum inundation depth and the maximum momentum flux.

Accordingly, the damage threshold for these facilities will depend on tank size and fill levels. Therefore, thresholds must be calculated and defined for each tank and filling state. For example, considering a cylindrical oil storage tank 10 meters high and 3 meters in diameter, and assuming the seawater density of $\rho = 1025\ kg/m^3$ and crude oil $\rho_{oil} = 850\ kg/m^3$, the resulting damage thresholds are presented in Table 4. For more details and the procedure for calculating the threshold values, please refer to the supplementary material.

Table 4. Description and definition of the proposed damage state function for a storage tank of 10 meters high and 3 meters in diameter, based on the stability equations for hydrodynamic loads.

DS	TIM	Fill level			Description
		Empty	Half full	Full	
Low	Max. Inundation depth (m)	$h \leq 1.0$	$h \leq 1.0$	$h \leq 1.5$	Low probability of significant structural damage, no significant damage 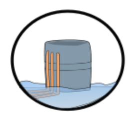
	Max. Momentum flux (m^3/s^2)	$hU^2 \leq 0.01$	$hU^2 \leq 0.03$	$hU^2 \leq 0.04$	
Medium	Max. Inundation depth (m)	$1.0 < h \leq 2.0$	$1.0 < h \leq 3.5$	$1.5 < h \leq 4.0$	Considerable probability of damage to pipes or minor deformation of non-structural components, with limited risk of loss of containment. 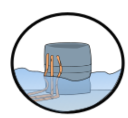
	Max. Momentum flux (m^3/s^2)	$0.01 < hU^2 \leq 0.06$	$0.03 < hU^2 \leq 0.08$	$0.04 < hU^2 \leq 0.13$	
High	Max. Inundation depth (m)	$h > 2.0$	$h > 3.5$	$h > 4.0$	High probability of major failure modes such as floating, sliding, overturning, or buckling, with a high risk of loss of containment and secondary consequences. 
	Max. Momentum flux (m^3/s^2)	$hU^2 > 0.06$	$hU^2 > 0.08$	$hU^2 > 0.13$	

© Author(s) 2026. CC BY 4.0 License.

4.2.4. Freight containers

Containers are a cornerstone of international maritime transport, as they account for 90% of global trade in goods (Bacigalupe and Hansz, 2023). However, because ports are typically located along coastlines, they are particularly exposed to severe tsunami impacts. Historical records highlight the high vulnerability of containerized cargo and storage systems. For instance, during the 2010 tsunami in Chile, around 700 containers located in storage yards were affected by flooding (Hou et al., 2022; Robertson et al., 2012), with structural damage to 30% of container stacks (Fritz et al., 2011). Another notable example is the 2011 Tohoku tsunami, which resulted in the displacement of over 3,000 containers, of which approximately 1,995 were completely lost (Kumagai, 2013).

Recent studies on damage thresholds have demonstrated significant methodological advances, although with limitations in specific applications, among which force-based modelling approaches stand out (Horspool and Fraser, 2016; Hou et al., 2022; Kumagai, 2013; Lee et al., 2024; Nistor et al., 2017; Robertson et al., 2012; Williams et al., 2019). These studies have shown that during flooding, containers are exposed to (i) horizontal displacement, (ii) buoyancy, and (iii) capsizing, causing them to collide with each other or with other parts of the port infrastructure. The magnitude of these forces depends on the maximum inundation depth, maximum flow velocity, and characteristics of the container, such as its weight and dimensions (Kumagai, 2013). Building on this framework, this study adopts a quantitative approach to assess the stability of standard Twenty-foot Equivalent Units (TEUs) under flooding conditions. Within this context, the critical instability thresholds for stacked freight containers exposed to tsunami-induced flooding were derived through a mechanics-based stability procedure considering two governing failure modes: flotation and sliding (see Figure 7).

For sliding, the procedure compared the horizontal tsunami-induced loading with the frictional resistance at the tank–foundation interface. The minimum force required to initiate the horizontal sliding of a container occurs when the driving force represented by the sum of hydrostatic F_{hs} and hydrodynamic drag F_d are greater than the resisting force F_{res} (See Eq. 4). The hydrostatic component F_{hs} is approximated as (Eq. 11):

$$F_{hs} = \frac{1}{2} * \rho * g * b_t * {h_{sub}}^2 \tag{11}$$

Where b_t is the Container length (12.19 m), h_{sub} is the maximum inundation depth. The drag force F_d, is calculated as (Eq. 12):

$$F_d = \frac{1}{2} * \rho * C_d * b_t * (h_{sub} - h_b) * U^2 \tag{12}$$

Where h_b is the elevation of the container base above the ground surface (0.14 m). The sliding failure condition is therefore defined as (Eq. 6). The velocity-dependent sliding solutions are subsequently approximated using a power-law relationship of the form $hU^2 = k$. The coefficient k is obtained through ordinary least-squares regression using the computed instability points. This allows the sliding maximum threshold (k) to be expressed directly in terms of momentum flux.

https://doi.org/10.5194/egusphere-2026-4720
Preprint. Discussion started: 14 August 2026
© Author(s) 2026. CC BY 4.0 License.

For a prescribed flow velocity, the critical inundation depth is obtained numerically by solving the equilibrium equation using a bisection algorithm. The numerical solutions indicate that the sliding threshold can be represented by a hyperbolic relationship between inundation depth and squared velocity.

The flotation maximum threshold is determined in a manner similar to that used for storage tanks, following the Eq. (8) and Eq. (9). The submerged volume was calculated for water levels exceeding the base clearance, and the critical flotation depth was defined as the inundation depth at which buoyancy equals the total downward weight of the container stack (Eq. 13):

$$h_{flot} = \frac{W_{FC}}{\rho * g * b_l * b_t} + h_b \qquad (13)$$

With b_l as the Container longitude (2.44 m). This threshold defines the onset of complete loss of vertical stability. Because the total weight (W) depends on the number of containers and their filling condition, flotation resistance increases with both stacking level and cargo mass (Cercone et al., 2017).

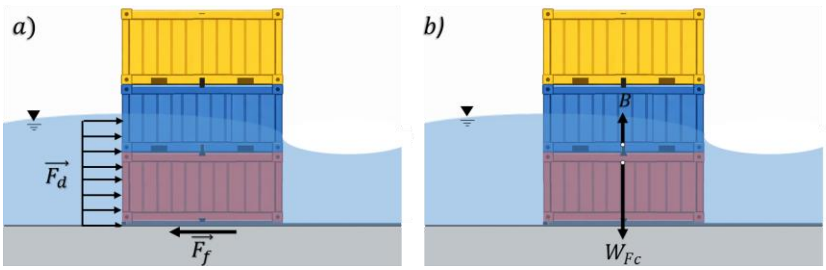

Figure 7. Stability diagram for stacking column of 3 containers. a) Hydrodynamic forces, and b) Buoyancy forces due to the impact of flooding caused by a tsunami.

Finally, the maximum flotation and sliding thresholds are translated into three damage states: DS1 for intensities below 30 % of the maximum instability threshold, DS2 for intensities between 30 % and 100 %, and DS3 for intensities exceeding the maximum threshold. The resulting damage-state functions are defined separately for empty and fully loaded containers and for each stacking level, providing threshold values based on maximum inundation depth and the hydrodynamic intensity measure $hU^2 = k$ where k is a filling-dependent sliding coefficient and is obtained by numerically solving the equilibrium equation using a bisection algorithm. Thus, the method provides a critical flotation depth, a critical sliding coefficient, and corresponding damage thresholds based on maximum inundation depth and the maximum momentum flux for integration into tsunami risk assessments at port scale.

Consequently, two-dimensional damage thresholds have been defined based on the possible instability mechanism. Table 5 provides a detailed description of the damage states for stacks of one to three containers, both empty and fully loaded conditions based on the aforementioned stability equations. For each combination of loading condition and stacking level, the total stack weight was calculated and used as the main stabilizing force. It should be noted that only damage associated with the onset of

https://doi.org/10.5194/egusphere-2026-4720
Preprint. Discussion started: 14 August 2026
© Author(s) 2026. CC BY 4.0 License.

instability is considered, whereas subsequent processes such as debris impact or cascading damage are not included. For more details and the procedure for calculating the threshold values, please refer to the supplementary material.

Table 5. Description of the proposed damage state function for empty and fully loaded containers, as well as for stacks of up to three different levels. Based on the stability equations for hydrodynamic loads.

DS	Filling	TIM	Stacking			Description
			1	3	5	
Low	Empty	Max. Inundation depth (m)	$h \leq 0.2$	$h \leq 0.5$	$h \leq 1.0$	The Flood does not generate significant movements. 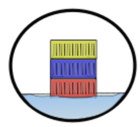
		Max. Momentum flux (m^3/s^2)	$hU^2 \leq 2.0$	$hU^2 \leq 3.0$	$hU^2 \leq 8.0$	
	Full	Max. Inundation depth (m)	$h \leq 1.0$	$h \leq 2.5$	$h \leq 4.0$	
		Max. Momentum flux (m^3/s^2)	$hU^2 \leq 15.0$	$hU^2 \leq 30.0$	$hU^2 \leq 80.0$	
Medium	Empty	Max. Inundation depth (m)	$0.2 < h \leq 0.3$	$0.5 < h \leq 1.0$	$1.0 < h \leq 1.5$	The tsunami could cause instability and damage to containers. Although it does not imply damage to the structure of the container, losses to the goods contained therein are estimated. 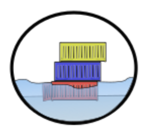
		Max. Momentum flux (m^3/s^2)	$2.0 < hU^2 \leq 2.5$	$3.0 < hU^2 \leq 5.0$	$8.0 < hU^2 \leq 12.0$	
	Full	Max. Inundation depth (m)	$1.0 < h < 1.2$	$2.5 < h < 3.5$	$4.0 < h \leq 5.5$	
		Max. Momentum flux (m^3/seg^2)	$15 < hU^2 \leq 20.0$	$30.0 < hU^2 \leq 60.0$	$80.0 < hU^2 \leq 99.0$	
High	Empty	Max. Inundation depth (m)	$h > 0.3$	$h > 1.0$	$h > 1.5$	There is a high probability of container column collapse. It is estimated that all 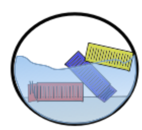
		Max. Momentum	$hU^2 > 2.5$	$hU^2 > 5.0$	$hU^2 > 12.0$	

https://doi.org/10.5194/egusphere-2026-4720
Preprint. Discussion started: 14 August 2026
© Author(s) 2026. CC BY 4.0 License.

	flux (m^3/s^2)				merchandise is lost, and debris has already begun.
Full	Max. Inundation depth (m)	$h > 1.2$	$h > 3.5$	$h > 5.5$	
	Max. Momentum flux (m^3/s^2)	$hU^2 > 20.0$	$hU^2 > 60.0$	$hU^2 > 99.0$	

4.2.5. Vehicles and Ro-Ro

Ports function as vehicle distribution centers, providing storage and pre-delivery processing for local and export markets (Supply Chain Management Review, 2025). The importation and exportation of vehicles through commercial ports generates significant economic value, making vehicle cargo particularly relevant for tsunami risk assessments. Throughout history, a significant number of tsunamis have caused substantial damage to vehicles in port facilities. However, the quantification of these losses may be limited in some cases (He et al., 2014). A notable example is the 2004 Indian Ocean tsunami, which had a substantial impact on the Port of Chennai, with an estimated economic loss of $2.5 million (Tang et al., 2006). The 2011 Tohoku tsunami in Japan also resulted in significant damage to vehicles in ports, with hundreds of cars and trucks destroyed in Sendai port (Suppasri et al., 2022), and 1,300 vehicles destroyed at Hitachi Port (Aftershocks shake Japan's auto industry, 2025).

Similarly to the previous asset, two modes of instability can be defined for static vehicles under tsunami hydrodynamic forces: buoyancy and sliding (Al-Qadami et al., 2024; Shah et al., 2019). Diverse experimental studies have provided quantifiable data on movement thresholds and hydrodynamic forces acting on vehicles under flood conditions. The findings of these studies provide a valuable dataset for the purpose of understanding vehicle stability. Experimental studies in controlled environments, have shown that a minimum inundation depth of 30 to 50 cm of is required for cars to initiate flotation, while sliding instability may occur once flow velocities exceed approximately 3.0 m/s (Martínez-Gomariz et al., 2018; Shah et al., 2021; Smith et al., 2017).

Based on these results, two-dimensional stability thresholds are proposed: inundation depth and depth-averaged flood velocity as explanatory variables (Al-Qadami et al., 2022; Cox et al., 2010; Martínez-Gomariz et al., 2018; Mustaffa et al., 2020; Russo et al., 2020; Shah et al., 2021; Smith et al., 2017). These parameters can be used to define damage states associated with the onset of flotation or sliding which may subsequently lead to additional damage. As illustrated in Table 6, the proposed thresholds are associated with the instability of vehicles and Ro-Ro within port environment, based on Martínez-Gomariz et al. (2019a). It is important to note that only damage associated with the onset of instability is considered, not any subsequent processes such as debris impact or cascading damage.

https://doi.org/10.5194/egusphere-2026-4720
Preprint. Discussion started: 14 August 2026
© Author(s) 2026. CC BY 4.0 License.

Table 6. Description and definition of damage state function for cars and other Ro-Ro. Obtained from Martínez-Gomariz et al. (2019a).

DS	TIM: Max. Inundation depth h (m)	TIM: Max. Momentum flux hU^2 (m^3/s^2)	Description	
Low	$h \leq 0.3$	$hU^2 \leq 0.9$	Minimal or no instability. The cars on display did not suffer any significant damage from the flooding.	
Medium	$0.3 < h \leq 0.5$	$0.9 < hU^2 \leq 1.9$	Some cars, such as those with low passenger capacity and sports cars, may be swept away by the flood.	
High	$h > 0.5$	$hU^2 > 1.9$	Cars exposed to flooding will be swept away due to complete loss of stability.	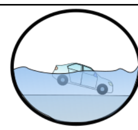

4.2.6. Pedestrians and port users

Pedestrians and port users are an integral part of port operations, including workers, passengers, and visitors who may be exposed to tsunami-induced flooding. Ensuring their safety is therefore a fundamental aspect of tsunami risk assessment in port environments. In 2023, the passenger port industry generated a total global economic impact of $168.6 billion and supported 1.6 million jobs worldwide (World Bank, 2023). Additionally, the global marina market was valued at approximately $10.49 billion in 2024, with projections to reach $15.51 billion by 2033 (Marinas Market Size, Share, Growth, and Industry Analysis, 2025).

Historically, numerous tsunamis have affected urban coastal areas, causing widespread destruction and significant loss of life (Synolakis and Kong, 2006), and ports have not been immune to these devastating events. During the 2004 Indian Ocean tsunami, the port of Chennai, India, recorded one fatality aboard a merchant ship, and five injuries among port employees (Takahashi et al., 2010). The same event also caused significant loss of life in the Maldives, resulting in 83 fatalities and 25 missing persons (Synolakis and Kong, 2006).

https://doi.org/10.5194/egusphere-2026-4720
Preprint. Discussion started: 14 August 2026
© Author(s) 2026. CC BY 4.0 License.

Given the limited availability of tsunami-specific human vulnerability models for port environments, existing research on pedestrian instability states and damage thresholds derived from river flooding studies provides a useful basis for assessing human vulnerability under tsunami-induced flooding. Simplified models of pedestrian stability consider slipping and tripping as the two main failure mechanisms under flood conditions (Martínez-Gomariz et al., 2016, 2020). A range of experimental studies have been conducted to assess the stability of pedestrians in floods, with a focus on TIMs such as inundation depth and flow velocity, establishing hydrodynamic thresholds associated with instability and injury (Cox et al., 2010; Martínez-Gomariz et al., 2016; Muhari et al., 2011; Russo et al., 2013; Shand et al., 2011).

These studies consistently identify maximum inundation depth and maximum flow velocity as the dominant factors governing instability, injury, and mortality. Based on this evidence, three pedestrian-stability thresholds are adopted to define a human safety state function proposed in this study (Table 7), following the classification criteria proposed by Martínez-Gomariz et al. (2016, 2019b).

Table 7. Description and definition of injury thresholds for a human safety state function for pedestrians. Obtained from (Martínez-Gomariz et al., 2016, 2019b).

DS	TIM			Description	
	Max. Inundation depth $\boldsymbol{h}$ ($\boldsymbol{m}$)	**Max. Flow velocity $\boldsymbol{U}$(m/s)**	$(\boldsymbol{h \cdot U})_{max}$ (m^2/s)		
Low	$h \leq 0.5$	$U \leq 1.0$	$(h \cdot U)_{max} \leq 0.16$	Minimal or no instability. Exposed individuals do not experience complications or significant stress due to flooding.	
Medium	$0.5 < h \leq 1.2$	$1.0 < U \leq 1.9$	$0.16 < (h \cdot U)_{max} \leq 0.22$	Pedestrians may encounter difficulties such as: slowness, occasional stumbling, and slipping when carrying out the evacuation protocol.	
High	$h > 1.2$	$U > 1.9$	$(h \cdot U)_{max} > 0.22$	People exposed to flooding will be swept away due to the complete loss of stability.	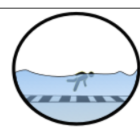

https://doi.org/10.5194/egusphere-2026-4720
Preprint. Discussion started: 14 August 2026
© Author(s) 2026. CC BY 4.0 License.

5. Tsunami Risk Assessment to port facilities

Following the UNDRR, disaster-risk framework, tsunami risk is defined as the potential for adverse consequences arising from the interaction between tsunami hazard and the exposure and vulnerability of port assets (UNDRR, 2025). In this final step, the results from the previous steps (hazard, exposure, and vulnerability) are combined. The proposed framework evaluates risk through two complementary perspectives (Martínez et al., 2022): an asset-specific approach, which captures the impact on individual assets, and an indicator-based approach, which provides an aggregated representation of relative risk levels across the port by aggregating indicator results into a risk index. It should be noted that the risk index derived in this study represents a comparative indicator of relative risk levels across docks, rather than an absolute quantification of expected physical damage or economic loss.

The primary objective of the tsunami risk assessment is to support decision-making by port managers and other stakeholders by providing a consistent representation of potential tsunami impacts. In line with international risk-management frameworks, such as the Sendai Framework for Disaster Risk Reduction (UNDRR, 2025), the proposed approach focuses on improving the identification and prioritisation of risk across port facilities from a prevention, mitigation, and preparedness perspective.

5.1. Specific-impact Approach

The asset-specific risk assessment is performed by combining the tsunami hazard with the vulnerability of each exposed port asset. For a given scenario, the maximum value of the selected TIM is extracted and compared against the vulnerability thresholds defined for the asset. When the intensity exceeds a given threshold, the corresponding Damage State (DS) is assigned, reflecting the physical and functional response of the asset (Goda and De Risi, 2024; Jelínek et al., 2011; Rafliana et al., 2022; UNDRR, 2025). Accordingly, within the proposed framework, the risk associated with a given asset is expressed as a function of three components: Hazard H, Exposure E, and Vulnerability V (Eq. 14).

$$R_{asset} = f(H, E, V) \tag{14}$$

The use of damage thresholds offers the advantages of traceability, interpretability, and risk communication, which are particularly relevant in operational planning and decision-making contexts. This approach is consistent with consequence-based risk matrices and assessment methodologies commonly applied in port management and natural-hazard risk analysis (Aguirre-Ayerbe et al., 2018; González-Riancho et al., 2014).

5.2. Integrated Risk Index

The Integrated Risk Index constitutes a relative and comparative measure, suitable for identifying priority areas and assets within the port, comparing different tsunami scenarios, and supporting decision-making in risk planning and management, thereby facilitating the prioritization of management and mitigation measures (Aguirre-Ayerbe et al., 2018; González-Riancho et al., 2014; Pilone and Demichela, 2018).

https://doi.org/10.5194/egusphere-2026-4720
Preprint. Discussion started: 14 August 2026
© Author(s) 2026. CC BY 4.0 License.

For this purpose, an **Integrated Risk Index** (IRI) is defined as a relative indicator suitable for comparing different port sections, tsunami scenarios, and asset configurations. The proposed framework requires the port area to be subdivided into management units, which constitute the spatial units of analysis. In the present study, docks are adopted as the management units for risk aggregation index IRI^{dock}

For each dock and asset type i, an *Asset Risk Indicator* ($ARI_i{}^{dock}$) is first computed by assigning increasing numerical values to the corresponding damage states. Accordingly, the number of elements of asset type i within each damage-state class j ($asset_i(DS_j)$) is aggregated and weighted as shown in Eq. (15).

$$ARI_i{}^{dock} = \sum asset_i(DS_1) \cdot 1 + \sum asset_i(DS_2) \cdot 2 + \cdots + \sum asset_i(DS_n) \cdot n \quad (15)$$

The **Integrated Risk Index** for a given dock (IRI^{dock}) is subsequently obtained by aggregating the relative contribution of each asset type to the overall port-wide damage burden. For this purpose, $ARI_i{}^{dock}$ is normalised by the corresponding Asset Risk Indicator calculated for the same asset type across the entire port ($ARI_i{}^{port}$), as shown in Eq. (16):

$$IRI^{dock} = \sum_{i=1}^{assets} \frac{ARI_i^{dock}}{ARI_i^{port}} \quad (16)$$

Where $ARI_i{}^{port}$ is obtained by summing all $ARI_i{}^{dock}$ values across docks for each asset type i.

This normalisation yields a relative *Integrated Risk Index* (IRI^{dock}) that reflects the concentration of tsunami-induced damage within a dock relative to the overall distribution of damage across the port. The resulting index is therefore suitable for comparing risk levels among docks, tsunami scenarios, and asset configurations.

Additionally, to identify which asset types are driving the risk levels within each dock, a normalised Asset Risk Indicator is computed using the Maximum Absolute Scaling Value (Eq. 17). This indicator is defined as the ratio between $ARI_i{}^{dock}$ and the maximum $ARI_i{}^{dock}$ value observed for the same asset type across all port docks.

$$ARI_{i\,max}^{Dock} = \frac{ARI_i^{dock}}{max(ARI_i{}^{dock})} \quad (17)$$

This normalization facilitates the identification of the asset types that contribute most to the risk level of each dock, allowing their relative importance to be compared across the port.

After obtaining the Integrated Risk Index, the relative risk values associated with each dock can be categorized into nominal risk classes. To define the thresholds separating these classes, objective classification methods, such as k-means clustering, Jenks natural breaks, or other data-driven discretization techniques, can be applied. This classification enables the transformation of the continuous IRI into relative risk levels, for example low, medium, and high, thereby improving the interpretability of the results and supporting the prioritization of docks according to their relative tsunami risk.

The main advantage of this approach lies in its ability to simplify the overall complexity of the risk assessment, facilitating the communication and interpretation of results through the standardization of outcomes into a single aggregate index (Abson et al., 2012). At the same time, the framework allows the aggregated risk index to be decomposed, enabling the contribution of

https://doi.org/10.5194/egusphere-2026-4720
Preprint. Discussion started: 14 August 2026
© Author(s) 2026. CC BY 4.0 License.

each exposed asset type to be individually assessed and mitigating the loss of information typically associated with index-based approaches. This supports port decision-makers in identifying the asset types that contribute most to risk within each dock, locating risk concentrations spatially, and understanding the factors influencing relative risk levels (Aguirre-Ayerbe et al., 2018).

6. Application of the Tsunami Risk Assessment Methodology to the Port of Cádiz (Spain)

In this section, the proposed methodology is implemented for the Commercial Port of Cádiz, under the jurisdiction of the Port Authority of the Bay of Cádiz (PABC). A probabilistic framework is adopted to evaluate the tsunami hazard (PTHA), illustrating the practical application of the proposed approach in a real port environment.

The tsunami risk assessment process is implemented through four main stages (see Figure 1). First, the port environment is characterised to identify relevant assets and cargo, which are spatially represented together with their main attributes. Second, tsunami hazard is assessed using a probabilistic approach based on regional seismic sources (NEAMTHM18 model), from which TIM maps are derived through hazard curves. Third, the static and dynamic exposure and vulnerability of the identified port assets are assessed. Finally, direct impacts are estimated by assigning representative damage state functions (DS), which are then aggregated to obtain dock-level and port-level risk indicators.

6.1. Port characterization.

The Port of Cádiz, located in southwestern Spain (Andalusia) on the Atlantic coast, in the Gulf of Cádiz (Figure 8), is a historic and strategically important port facility serving commercial shipping as well as industrial, logistics, and passenger activities. This port plays a significant role in Spain's port system, as a key logistics hub for freight traffic, naval activities, and passenger transport. Its operations contribute directly to the economic development of the Iberian Peninsula and to Spain's foreign trade, particularly through connections with Africa, the Americas, and the European Atlantic Arc.

The port's location is prone to tsunami impacts due to its proximity to the seismically active and tsunamigenic region of the southwestern Iberian margin (Aguirre-Ayerbe et al., 2025; González et al., 2021). This offshore zone, situated roughly 400 km from Cape São Vicente, was the source of the historic 1755 Lisbon earthquake and its associated tsunami (Garcia-Orellana et al., 2006; Lario et al., 2011; Lima et al., 2010). The tidal regime is mesotidal, with a tidal range of 4 m (González et al., 2021), which constitutes a relevant factor for port operations and planning.

https://doi.org/10.5194/egusphere-2026-4720
Preprint. Discussion started: 14 August 2026
© Author(s) 2026. CC BY 4.0 License.

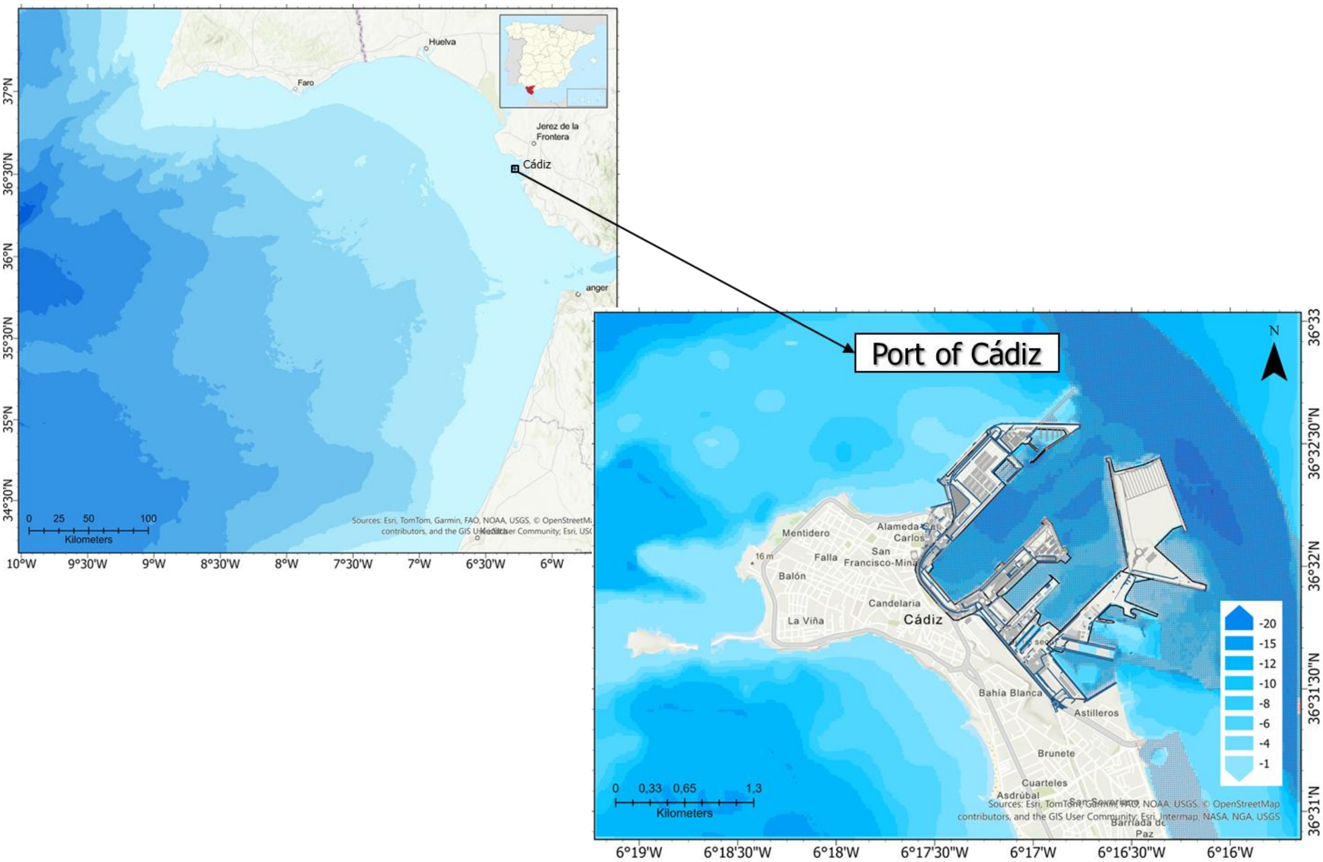

Figure 8. On the left is the bathymetry of the Gulf of Cádiz and the location of the Port of Cádiz on the southwestern coast of Spain. On the right is the port's plan view, showing the locations of the sampling points used in the bathymetric survey conducted by the port. Basemap sources: Esri, TomTom, Garmin, FAO, NOAA, USGS, © OpenStreetMap contributors, and the GIS User Community. Intermap, NASA, NGA| Powered by Esri.

Bathymetric data were compiled, including the GEBCO databases for the Atlantic Basin, the EMODNET database for the Gulf of Cádiz, and nautical charts 4430 and 443B for detailed coastal information, supplemented by a dedicated bathymetric survey carried out by the Port of Cádiz. Additionally, topographic data were obtained from high-resolution digital elevation models (2 m resolution) derived by interpolation from the terrain class of LIDAR surveys conducted under the National Aerial Orthophotography Plan (PNOA).

The regional deep-sea bathymetry is relatively smooth, with no significant geomorphological features, such as submarine canyons, that could affect tsunami-wave propagation. In contrast, the Cádiz harbour has a relatively shallow bathymetry. The port has been dredged to a depth of approximately 14 meters below the local mean sea level, enabling the safe entry of large vessels.

https://doi.org/10.5194/egusphere-2026-4720
Preprint. Discussion started: 14 August 2026
© Author(s) 2026. CC BY 4.0 License.

A comprehensive dataset was compiled from the port's layout plan, describing the spatial configuration of docks and the distribution of primary facilities. The port comprises a range of docks, primarily designed to accommodate container traffic, Ro-Ro, cruise ships, general cargo, and specialised cargo (see Figure 9). These facilities support a wide range of commercial activities, including agri-food bulk transport, general cargo operations, and tourist traffic.

The port has approximately 4.5 km of wharf length and nearly 1 million square meters of landside operational area. It comprises several basins with distinct operational functions, including the Commercial Basin, which accommodates container cargo, general cargo, passengers, and Ro-Ro traffic; the Fishing Basin, used for the storage of seafood and other refrigerated goods; and the Dry Dock Basin, dedicated primarily to ship-repair activities. In addition, the port includes a dock designated for recreational vessels, known as Puerto América dock (see port description and uses in Table 8).

Table 8. Description of the docks within the port and their uses.

Basin	Dock	Usage	Length (m)	Total area (m^2)
Commercial Basin	Reina Sofía	Conteiner	640	138000
	Alfonso XIII	Passengers	180	37000
	Ciudad & Reina Victoria	Passengers	522	41700
	Marqués de Comillas	Ro-Ro and general cargo	636	99750
	De La Libertad	Ro-Ro and general cargo	304	81000
Fishing Basin	G. Fernandez Ladreda	Fishing	340	39500
	Lonja	Fishing	166	41700
	Levante	Fishing and diesel fuel	150	38450
Dry Dock Basin	Embocadura	Shipyard	110	70500
	Armamento	Shipyard	200	61200
Other Docks	Puerto América	Marina	690	95000

The available data indicate that the port handles a minimum of approximately 32,000 TEUs per year, of which around 40% correspond to empty containers. Container stacks range from 1 to 5 levels in height and are primarily located at the Reina Sofia and La Libertad docks (Figure 10). Ro-Ro traffic consists predominantly of vehicles (92%) mainly concentrated at the Marqués de Comillas and La Libertad docks, with the remaining share corresponding to other goods transported in Ro-Ro containers. Passenger traffic over the last 3 years has averaged approximately 690,000 passengers per year. At least one cruise ship is berthed at the passenger terminals around 50% of the time, using mobile ramps for boarding and disembarkation. Storage tanks located within the port are used for diesel fuel storage and are located at the Levante and Armamento docks. Table 9 summarises the inventory of port assets considered in this case study.

https://doi.org/10.5194/egusphere-2026-4720
Preprint. Discussion started: 14 August 2026
© Author(s) 2026. CC BY 4.0 License.

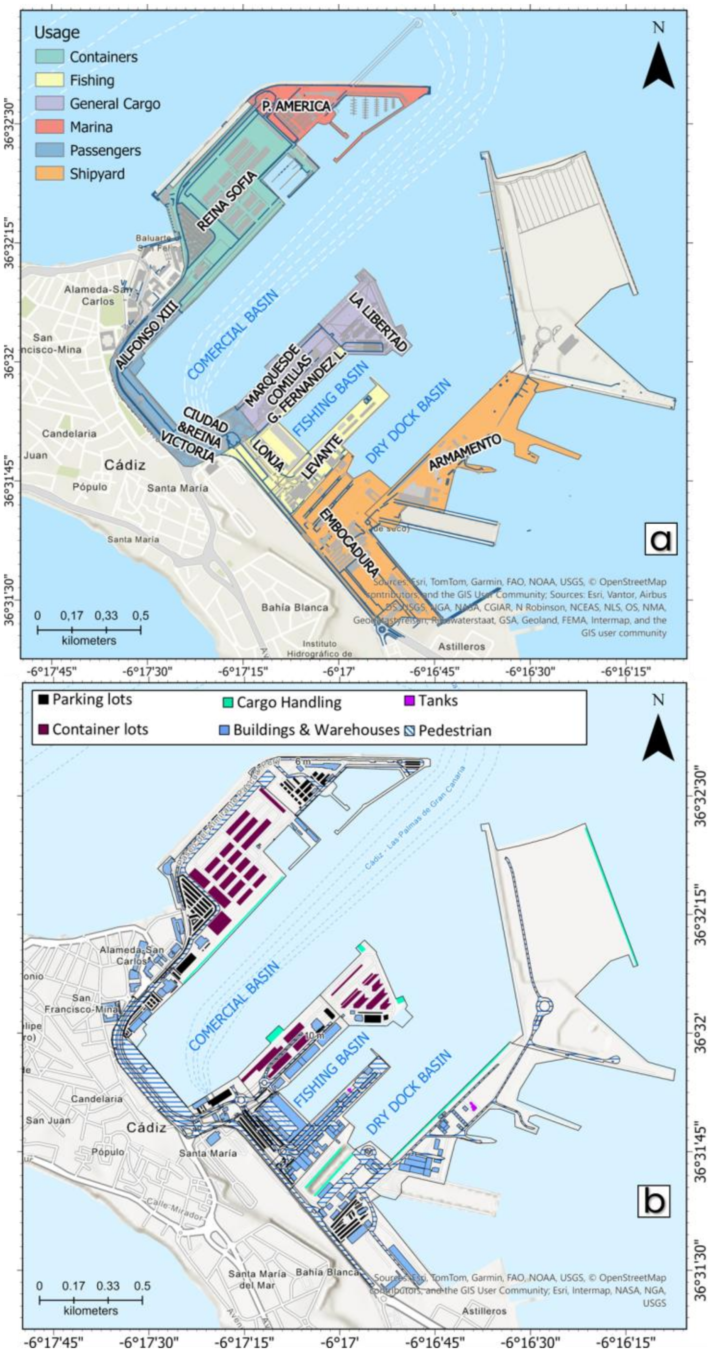

Figure 9. Plan of the port and its docks, with the respective commercial operations delineated in a color-coded system shown on (a). On (b) is shown the spatial distribution of the main assets located within the port. Base map sources: Esri, TomTom, Garmin, FAO, NOAA, USGS, © OpenStreetMap contributors, and the GIS User Community. Intermap, NASA, NGA| Powered by Esri.

https://doi.org/10.5194/egusphere-2026-4720
Preprint. Discussion started: 14 August 2026
© Author(s) 2026. CC BY 4.0 License.

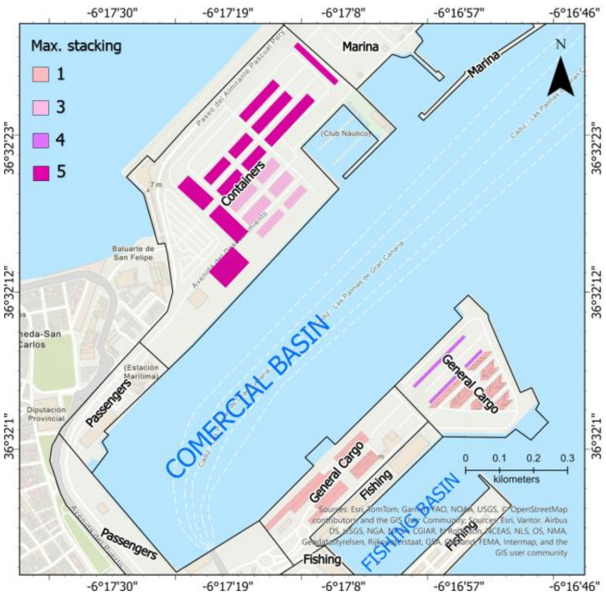

Figure 10. Location of the containers in the port. The colours indicate the maximum number of containers that can be stacked. Base map sources: Esri, TomTom, Garmin, FAO, NOAA, USGS, © OpenStreetMap contributors, and the GIS User Community. Intermap, NASA, NGA| Powered by Esri.

6.2. Tsunami Hazard Assessment

A probabilistic framework is adopted in this case study to assess tsunami hazard (PTHA), allowing the consideration of epistemic uncertainties. The tsunami hazard assessment focuses on the characterisation of tsunami-generating events and their potential impact on the port, including tsunami generation, propagation, and inundation within port facilities. A seismotectonic analysis of the sources capable of generating tsunamis affecting the port is first carried out using the NEAMTHM18 model (Basili et al., 2021), resulting in a catalogue of representative seismic scenarios. These seismic scenarios are subsequently simulated numerically to derive tsunami hazard curves and the corresponding TIM maps for the port's landside area.

6.2.1. Characterization of tsunami-generating sources

To characterise the earthquake sources relevant for the hazard assessment, outputs from the NEAMTHM18 regional tsunami model were employed (Basili et al., 2019, 2021). This model provides a probabilistic characterisation of seismotectonic sources within a S-PTHA framework across the NEAM region, encompassing the northeastern Atlantic, the Mediterranean, and adjacent seas. It includes the estimation of annual occurrence rates for a large number of potential seismic events, accounting for multiple source configurations and epistemic uncertainty.

Based on the NEAMTHM18 framework local, regional, and distant tsunamigenic sources relevant to the study area were identified and selected. The seismicity is classified into different types depending on the level of knowledge of the underlying

https://doi.org/10.5194/egusphere-2026-4720
Preprint. Discussion started: 14 August 2026
© Author(s) 2026. CC BY 4.0 License.

data, distinguishing preliminarily between predominant seismicity (PS), associated with well-characterised faults capable of generating large-magnitude earthquakes, and background seismicity (BS), characterized by higher uncertainty (Selva et al., 2016). Additional source types are defined in NEAMTHM18 through adaptations that consider source-to-coast distance and the number of fixed parameters adopted in the seismicity models (like SBS as secondary BS, PSMar as PS in the Mid-Atlantic Ridge, and PSSlip as PS due to slippage (Basili et al., 2019).

This classification resulted in a large set of seismic scenarios (on the order of $5x10^5$), including both near-field sources (BS, SBS) and distant sources (PSMar, BSDistant, and PSSlip), as shown in Figure 11. The model further incorporates Bayesian alternative branches to represent uncertainty in frequency–magnitude relationships, particularly affecting annual occurrence rates and distribution tails.

Given the large number of scenarios generated, a disaggregation process was applied following the methodology of Gibbons et al. (2020) and Power et al. (2018). Three Points of Interest (PoIs) located in the vicinity of the port were selected from the NEAMTHM18 model (Figure 11). From the initial scenario set, those contributing most significantly to the hazard curve at the selected PoIs were retained, subject to the criterion that their cumulative contribution reproduces at least 99 % of the original regional hazard curve (Figure 11).

This process resulted in an optimized set of seismic scenarios for local sources (4.8×10^3 for BS, 2.2×10^3 for SBS) and distant sources (1.8×10^2 for PSMar, 7×10^2 for BSDistant, and 8.9×10^2 for PSSlip). For each scenario, the seismic parameters required for tsunami simulation, together with the corresponding annual occurrence rates, were obtained from the NEAMTHM18 regional model (Basili et al., 2019, 2021).

https://doi.org/10.5194/egusphere-2026-4720
Preprint. Discussion started: 14 August 2026
© Author(s) 2026. CC BY 4.0 License.

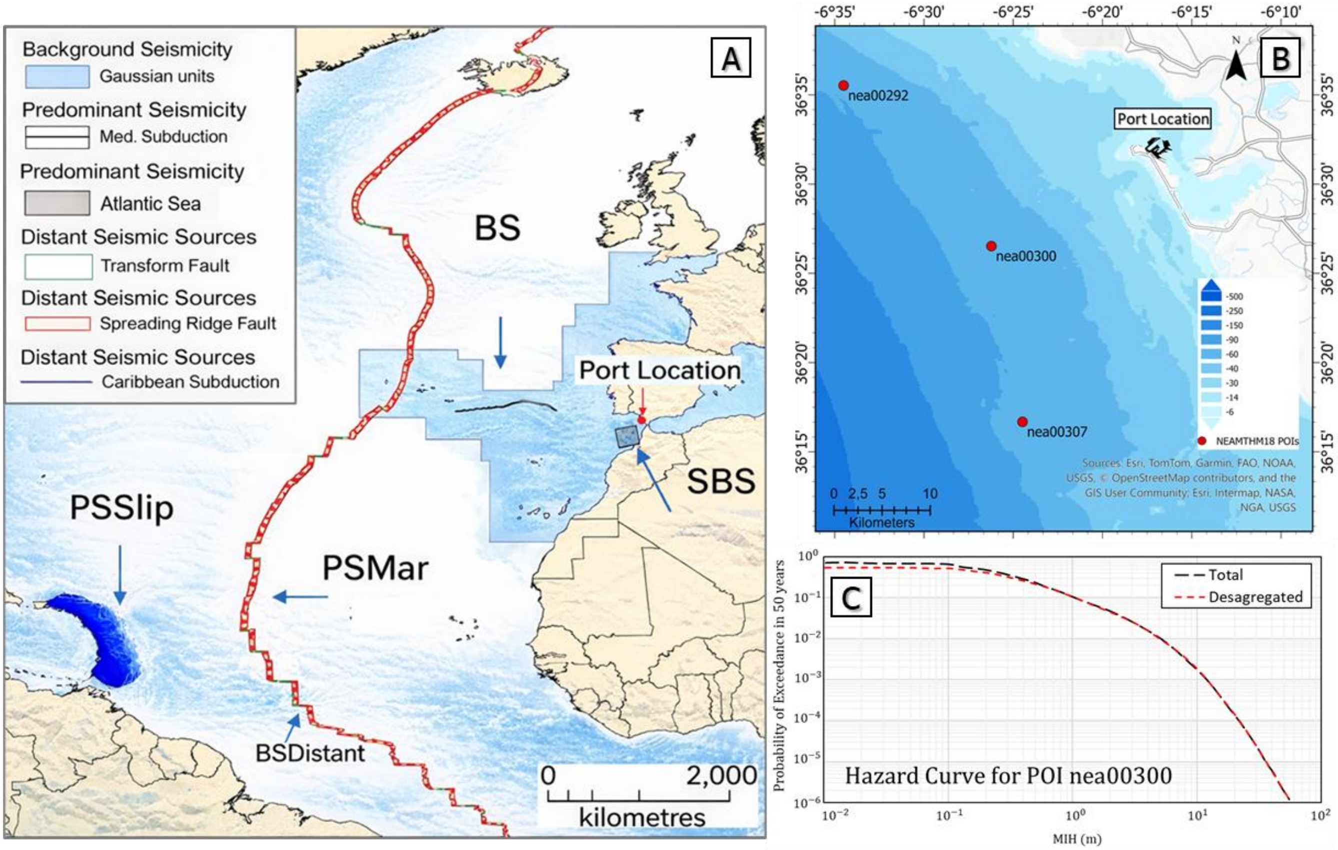

Figure 11. A. Locations of the seismic sources Background Seismicity (BS), Special BS (SBS) and Predominant Seismicity (PS), obtained from NEAMTHM18. B. Locations of Points of Interest (PoIs), used to retrieve the NEAMTHM18 results, based on Basili et al. (2021). C Hazard curve extracted from the PoI nea00300 indicating the probability that a given flood depth will be exceeded in 50 years, with MIH as Maximum flood depth (see Tonini et al. (2021)). The dashed black line represents the original cumulative hazard curve, and the red line corresponds the 99% of the total hazard curve based on the subset of selected scenarios (Disaggregated). Base map sources for A and B: Esri, TomTom, Garmin, FAO, NOAA, USGS, © OpenStreetMap contributors, and the GIS User Community. Intermap, NASA, NGA| Powered by Esri.

6.2.2. Tsunami numerical simulation

The complexity of PTHA necessitates the appropriate discretisation of thousands of source scenarios and high-resolution hazard modelling (Basili et al., 2021; Gibbons et al., 2020). When considering the full range of approaches, NLSWE models (e.g. Tsunami HySEA, COMCOT or MOST) are shown to be the most suitable option for PTHA-type studies in the port's landside area. The capacity to conserve mass and momentum in a stable manner, the robustness to discontinuities (e.g., wetting–drying schemes), and the efficiency in operating with very high-resolution grids render them particularly suitable for evaluating a large number of scenarios in complex domains (Behrens and Dias, 2015; Gibbons et al., 2020; González et al.,

https://doi.org/10.5194/egusphere-2026-4720
Preprint. Discussion started: 14 August 2026
© Author(s) 2026. CC BY 4.0 License.

2022; Macías et al., 2020a, b). Furthermore, they facilitate the incorporation of friction and structures without a substantial increase in computational cost, a fundamental aspect in hazard analysis that necessitates thousands of simulations.

The GPU-based numerical model Tsunami-HySEA (Macías et al., 2017) was applied to simulate the tsunami generation, propagation and inundation within the port. Simulations were performed on the Leonardo Tier-0 high-performance computing cluster at CINECA (Italy) enabling the execution of large ensembles of scenarios through parallel GPU processing. During the generation phase, the model applies Okada's analytical solutions (Okada, 1985) to estimate the coseismic seafloor displacement and the resulting initial sea surface deformation. Tsunami propagation is subsequently simulated by solving the NLSWE using a finite volume numerical approach. The model also allows the incorporation of multiple fault planes, enabling the representation of complex rupture scenarios. Comparative studies have demonstrated that NLSWEs are capable of accurately reproducing inundation depths and currents (Arcos and LeVeque, 2015; Brocchini, 2013; Lynett et al., 2017; McCabe et al., 2014; Son et al., 2011). Consequently, it is common practice to use NLSWE models within PTHA frameworks (Aguirre-Ayerbe et al., 2025; Gibbons et al., 2020; Glimsdal et al., 2019; González et al., 2022, González et al., 2021; Tonini et al., 2021).

Regarding the reference datasets used in the numerical simulations, a system of five nested computational grids was used. At the global and regional scales, the grid resolution is on the order of ~1 km, while at the local scale it reaches approximately 5 m, allowing tsunami inundation to be resolved at port scale (Figure 12). GEBCO data were used for the coarser grids (levels 1 and 2), whereas the regional grids covering the Gulf of Cádiz were refined using the EMODnet database (levels 3 and 4). The highest resolution grid (level 5) was supplemented with nautical charts and a detailed bathymetric survey conducted by the local port authority. To ensure consistency among the different datasets, all bathymetric and topographic information was referenced to the mean-sea level vertical datum defined by the local tide gauge.

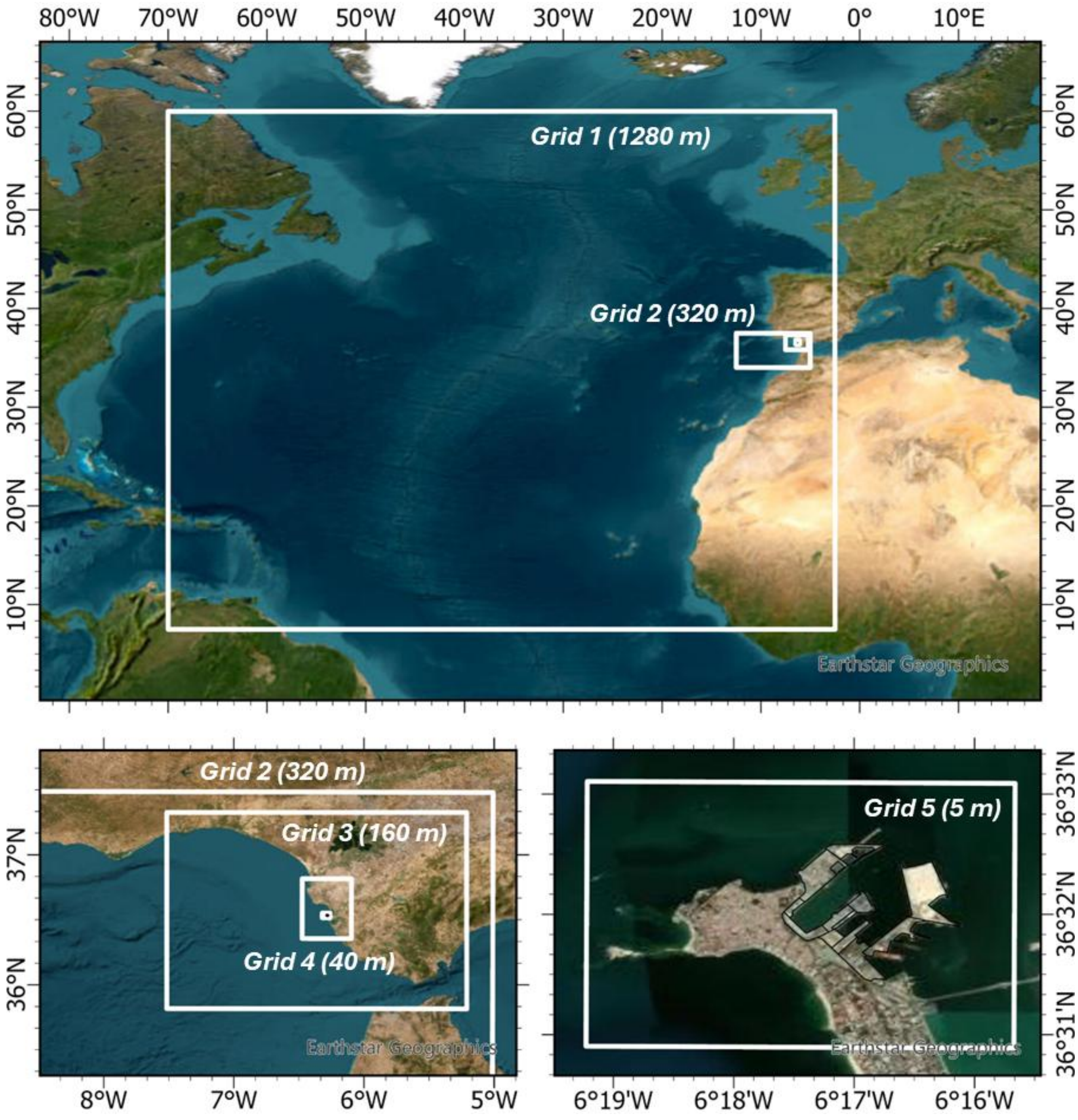

820 **Figure 12. Schematic diagram of the 5 nested grids used for the numerical tsunami simulations. The base map was designed and developed by Esri | Powered by Esri.**

For each simulated scenario in which the inundation depth exceeds 1 cm, the maximum values of three TIM —flow depth (m), velocity (m/s), and momentum flux (m^3/s^2)—are recorded at each node of the finest grid covering the port's landside area. Based on these results, node-specific hazard curves are constructed (Figure 13), relating the exceedance probability of the

https://doi.org/10.5194/egusphere-2026-4720
Preprint. Discussion started: 14 August 2026
© Author(s) 2026. CC BY 4.0 License.

selected TIM to the occurrence rates of the contributing tsunami scenarios over a 50-year exposure period. Epistemic uncertainty is represented through the 98th percentile curves.

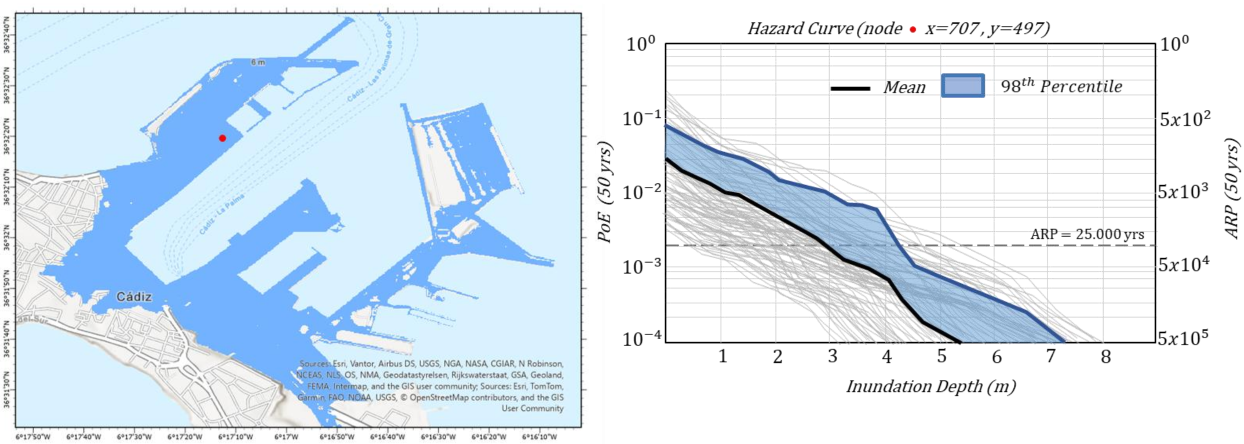

Figure 13. On the left is a map of the flooded area (in blue) in the port and the right side shows the Hazard Curve at a node in the finer grid (red dot) located within the port's landside operational Area. Basemap sources: Esri, TomTom, Garmin, FAO, NOAA, USGS, © OpenStreetMap contributors, and the GIS User Community. Intermap, NASA, NGA | Powered by Esri.

The result of this process is a TIM map in which, for each grid node, the probability of exceedance (PoE) or the corresponding Average Return Period (ARP) of the maximum TIM values over a 50-year window time is defined. This methodology enables the generation of probabilistic maps of a given TIM for a specific average return period and epistemic uncertainty percentiles. Figure 14 presents the probabilistic hazard results for the port's landside operational area corresponding to a 25000-year ARP shown for the 98th percentile. These return period and percentile (98th) values were approved by the City Council authority and correspond to the design criteria adopted for the preparation of tsunami evacuation maps in the Cádiz region (Aguirre-Ayerbe et al., 2025).

https://doi.org/10.5194/egusphere-2026-4720
Preprint. Discussion started: 14 August 2026
© Author(s) 2026. CC BY 4.0 License.

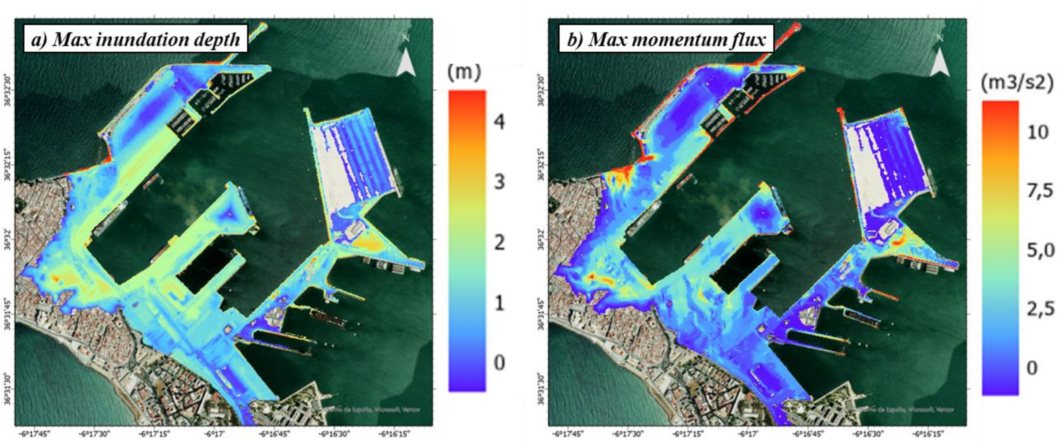

Figure 14. Probabilistic tsunami hazard maps for 25000-year ARP scenario and 98th percentile. Maps a and b show the maximum inundation depth and the maximum momentum, respectively. The base map sourse: © Plan Nacional de Ortofotografía Aérea (PNOA) - Instituto Geográfico Nacional. Spain, 2025.

6.3. Exposure and Vulnerability Assessment of the Port of Cádiz key assets

The main port assets located at each dock were identified following the subdivision of the landside operational area shown in Figure 9, in coordination with the port's risk managers. Using the port layout plan provided by the PABC, an inventory of the maximum number of assets at dock level was compiled (Table 9), together with the calculation of the Exposure Index EI^{dock} for each dock, following Eq. (1). The results of the analysis were presented using Jenks' "natural breaks" classification, which is a data clustering method that aims to create clusters with very similar values within each cluster, while maximizing the differences between distinct clusters. Figure 15 illustrates the spatial distribution of exposure for the main asset categories across the port. This representation allows the location of assets within the landside operational area to be identified and provides a clear indication of relative exposure levels across the docks.

Table 9. Inventory of maximum number of items displayed for each dock in the port of Cádiz.

Dock	Vehicles & Ro-Ro	Buildings & Warehouses	Container lots	Tanks	Cargo Handling	Pedestrian area (m2)	EI^{dock}
Puerto América	337	5	-	-	-	17758	0,264
Alfonso XIII	319	4	-	-	-	6350	0,184
Ciudad & Reina Victoria	128	8	-	-	-	47513	0,384
La Libertad	22	3	267	-	2	-	0,413

© Author(s) 2026. CC BY 4.0 License.

G. Fernandez Ladreda	-	5	-	-	-	-	0,045
Lonja	447	4	-	-	-	20250	0,308
Levante	55	25	-	3	-	21033	0,575
Embocadura	532	19	-	-	2	24723	0,783
Armamento	-	28	-	11	1	14145	1,258
Marqués de Comillas	69	1	248	-	1	7106	0,303
Reina Sofía	920	10	2353	-	1	18547	1,482
Total	2829	112	2868	14	7	177426	6

The results indicate that the Reina Sofia and Armamento docks exhibit the highest exposure levels within the port terminal, driven respectively by the high concentration of container storage areas and the presence of warehouses and buildings. These are followed by the Embocadura dock, characterised by a high number of parking areas and buildings. Lower, but still significant exposure levels are observed at the Levante, La Libertad, and Ciudad & Reina Victoria docks. Together, these six docks account for more than 80% of the total exposure inventory of the port.

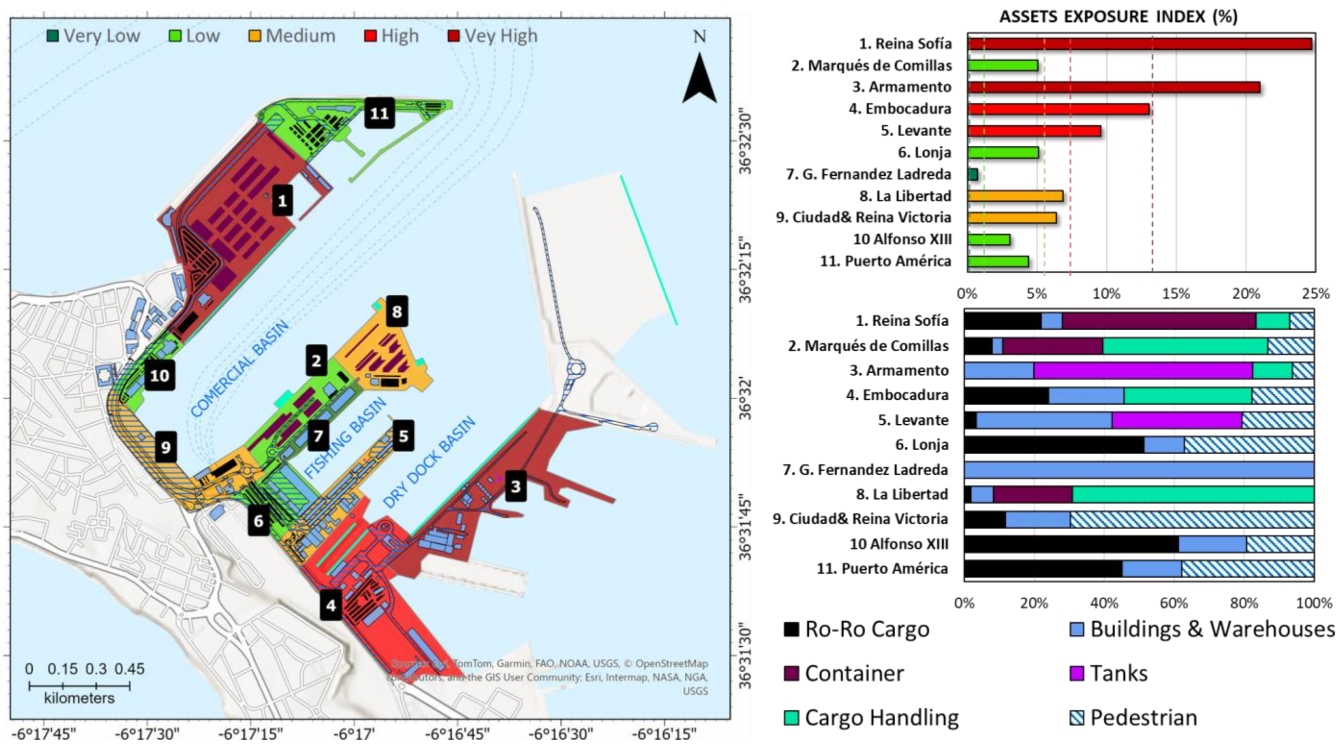

https://doi.org/10.5194/egusphere-2026-4720
Preprint. Discussion started: 14 August 2026
© Author(s) 2026. CC BY 4.0 License.

Figure 15. The map showing the port's infrastructure and the ranking of its docks. The classification of the nominal exposure levels of the docks was performed using Jenks' natural break method. Five classes were determined based on the results of the Exposure Index (EI), ranging from very low to very high. Basemap sources: Esri, TomTom, Garmin, FAO, NOAA, USGS, © OpenStreetMap contributors, and the GIS User Community. Intermap, NASA, NGA | Powered by Esri.

A static exposure framework was adopted for assets whose configuration can be assumed to remain constant over time, including, warehouse facilities, buildings, ramps/cranes and pedestrian areas. In contrast, a dynamic exposure formulation was applied to goods-related assets, such as storage tanks, containers, vehicles and other Ro-Ro, in order to capture their inherent temporal variability. The implementation of the exposure model was conditioned by the availability of asset-specific operational data within the Port of Cádiz. Accordingly, the formulation incorporates: (i) average annual occupancy rates in vehicle storage areas; (ii) discrete fill states for diesel storage tanks (empty, half-full, and full); and (iii) container stacking capacity and the average annual proportion of empty units (TEUs). Together, these parameters enable a more realistic representation of exposure conditions within the port operational environment.

A Monte Carlo approach was implemented to support the probabilistic characterization of dynamic exposure, integrating occupancy rates and container stacking distributions to generate a large number of stochastic exposure realizations within the port system. Variations in spatial arrangement and loading conditions directly influence asset susceptibility to tsunami-induced hydrodynamic impacts.

Discrete uniform probability distributions were assigned to both stacking configuration and loading condition (loaded/empty) for dynamically exposed elements such as containerized cargo. This assumption was applied across the port domain, while accounting for spatial heterogeneity in stacking capacity, as maximum allowable stacking varies between terminal areas (Figure 10). Incorporating this constraint is essential for realistically reproducing operational conditions and adequately representing the intrinsic variability of port environments within the probabilistic framework.

The resulting exposure characterization constitutes a key input for the vulnerability assessment, as the defined asset states and occupancy conditions are directly linked to tsunami-induced damage mechanisms and the associated fragility functions. The vulnerability of the exposed assets was assessed according to the methodology described in Sect. 4.2, where asset-specific damage-state functions were defined for the main assets.

6.4. Tsunami risk assessment in the port of Cadiz

The tsunami risk assessment was conducted using the two complementary perspectives defined in the proposed framework: (i) a specific-impact approach, which evaluates the consequences for individual assets; and (ii) an Integrated Risk Index (IRI), which provides an aggregated representation of relative risk levels at dock level.

The specific-impact risk assessment for port assets was conducted using an integrated framework combining hazard, exposure, and fragility components. The selected hazard scenario corresponds to 25000-years ARP (98th epistemic uncertainty percentile), representing an extreme yet plausible event according to the probabilistic hazard assessment conducted for the municipality of Cádiz. This scenario also corresponds to the design parameters officially adopted by the City Council for

https://doi.org/10.5194/egusphere-2026-4720
Preprint. Discussion started: 14 August 2026
© Author(s) 2026. CC BY 4.0 License.

emergency and evacuation planning (Aguirre-Ayerbe et al., 2025). Given the discrete nature of the damage states defined for each asset in the vulnerability assessment, risk results were represented using the ordinal risk classification defined in the proposed framework. Figure 16 illustrates the resulting spatial distribution of specific-impact risk across the main asset categories within the port.

The results reveal marked spatial and functional variability in tsunami risk across the port, driven by the combined influence of asset-specific vulnerability and temporally varying exposure conditions. More than 55% of the analysed assets fall within high-risk categories. Storage tanks are entirely classified within high-risk areas, while high-risk levels are reached by 99% of pedestrian areas, 65% of vehicles and Ro-Ro, 53% of container yards, and approximately 30% of cargo transfer areas. In contrast, nearly 90% of buildings and warehouses remain within low-risk levels.

These results illustrate how asset-specific vulnerability and exposure conditions influence the spatial distribution of tsunami risk within the port. The approach helps identify critical assets and priority areas that may require more detailed assessment, targeted mitigation measures, or specific emergency-planning actions.

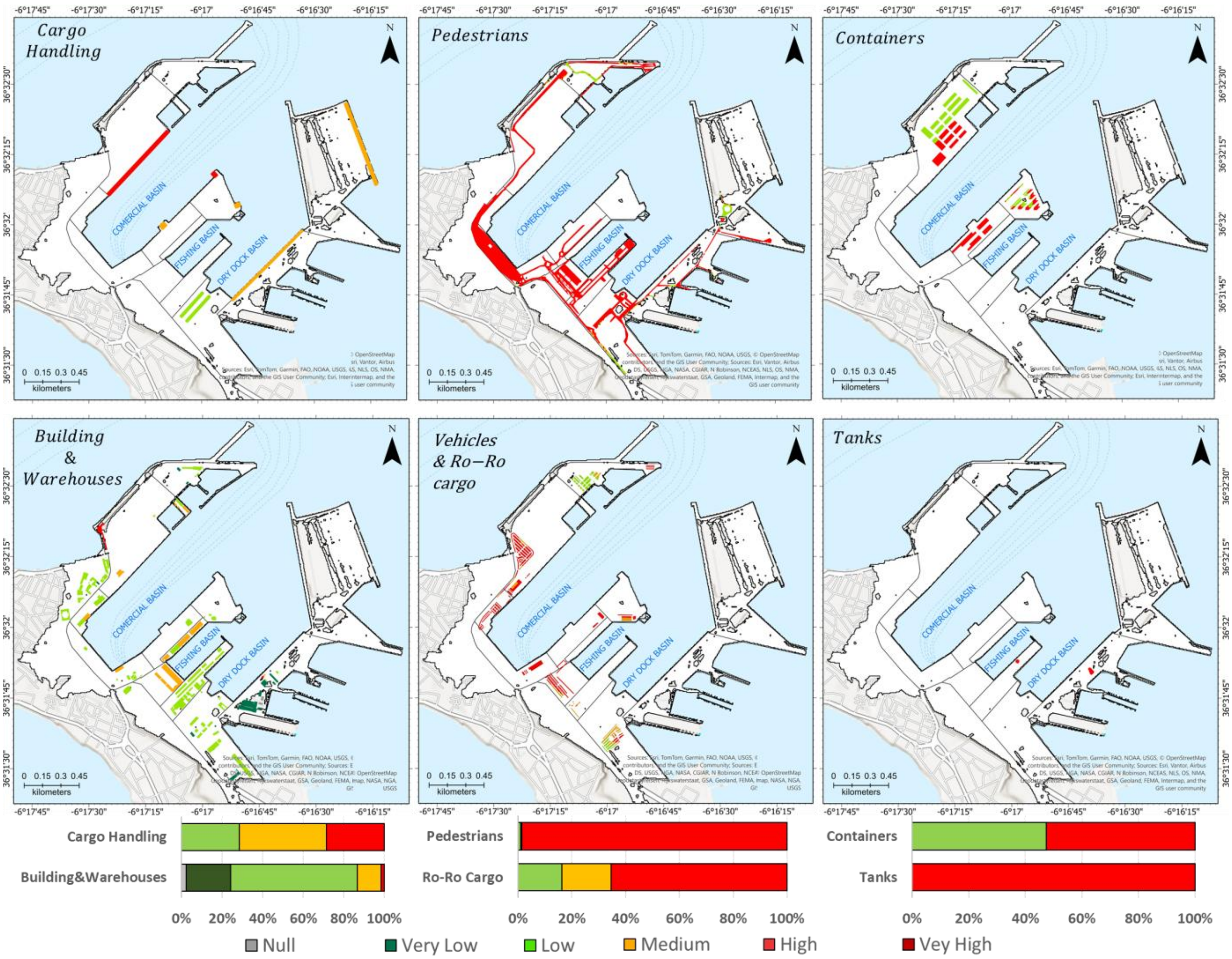

Figure 16. Risk levels to the key assets (Buildings, Ro-Ro, containers, cargo handling equipment, pedestrians, and storage tanks), related to the specific-impact resulting from a 25 000-year return period ARP hazard scenario (98th percentile). The extent of the flood depth layer for hazard scenario is shown in white. The bars at the bottom of the figure show the percentage of every damage state for each asset assessed. Basemap sources: Esri, TomTom, Garmin, FAO, NOAA, USGS, © OpenStreetMap contributors, and the GIS User Community. Intermap, NASA, NGA | Powered by Esri.

The Integrated Risk Index (IRI^{dock}), was used to assess the relative risk levels across the docks that constitute the port facility (Figure 17). The IRI^{dock} accounts for both the risk level associated with individual asset types, and the number of assets assigned to each damage state within a dock. Following the approach used in the Exposure Index, Jenks' classification of "natural breaks" has been used to generate five nominal risk levels. This aggregation enables the identification of docks with the highest relative risk under the selected probabilistic hazard scenario. In turn, it facilitates the identification of asset types contributing most to the relative risk level of each dock.

https://doi.org/10.5194/egusphere-2026-4720
Preprint. Discussion started: 14 August 2026
© Author(s) 2026. CC BY 4.0 License.

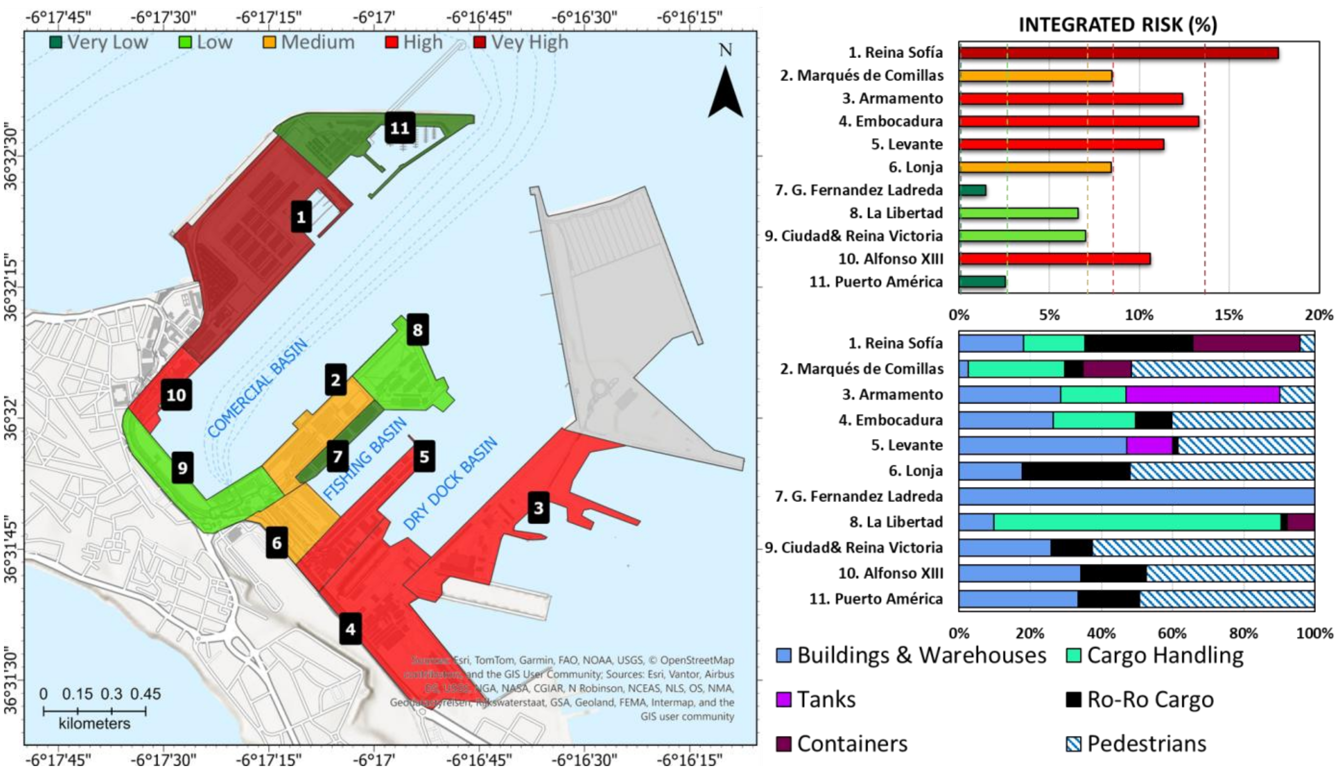

Figure 17. IRI results for a 25000-year ARP hazard scenario (98th percentile) are shown on the left. The upper right panel shows the resulting risk index map for each dock and the lower right illustrate the percentage values by dock and the relative number of assets covered in each dock. The classification of the nominal Integrated risk levels of the docks was performed using Jenks' natural break method. Five classes were determined. Basemap sources: Esri, TomTom, Garmin, FAO, NOAA, USGS, © OpenStreetMap contributors, and the GIS User Community. Intermap, NASA, NGA | Powered by Esri.

The results indicate that the Reina Sofia dock presents the highest tsunami risk, primarily due to the concentration of container storage area, Ro-Ro cargo, and buildings & warehouse facilities. The docks classified as high-risk (Armamento, Embocadura, Levante, and Alfonso XIII) derive a substantial proportion of their risk from pedestrian areas, buildings & warehouses, which together account for more than 60% of the overall risk score. In contrast, docks dedicated mainly to passenger traffic exhibit lower overall risk values. However, these areas also contain the largest zones designated for pedestrian use, where more than 95 % of the assessed surfaces fall within high-risk categories for human safety.

These findings demonstrate that tsunami risk within the port is not uniformly distributed, but strongly depends on the combination of asset type, operational use, and exposure conditions. The adopted approach enables the identification of critical docks and asset types, as well as the configurations that drive high risk levels.

https://doi.org/10.5194/egusphere-2026-4720
Preprint. Discussion started: 14 August 2026
© Author(s) 2026. CC BY 4.0 License.

The adopted IRI is not intended to replace detailed hydrodynamic or asset-level risk assessments, but rather to complement them by providing a synthetic and comparative representation of tsunami risk. This facilitates the comparison of risk levels across docks and supports the interpretation of spatial and functional risk patterns within the port system.

7. Discussion

The methodological framework presented in this study addresses a fundamental gap in coastal engineering and port planning: the application of tsunami risk assessment to structured, asset-specific decision-making tools. This approach spatializes the port's landside operational area into discrete operational units, analyzing the various hydrodynamic failure mechanisms of its critical assets.

One aspect that deserves discussion concerns the suitability of the hydrodynamic model used for tsunami hazard assessment within port environments. While Boussinesq-type models may better represent frequency dispersion, harbour resonance, and complex circulation patterns in sheltered waters, the proposed framework relies on the NLSWE-based Tsunami-HySEA model due to its computational efficiency and suitability for large-scale PTHA applications involving thousands of scenarios. To evaluate the implications of this modelling choice, an illustrative comparison was performed between Tsunami-HySEA and the Boussinesq-type model FUNWAVE-TVD using a deterministic tsunami scenario generated by the combined activation of the Horseshoe Fault (HSF) and the Marqués de Pombal Fault (MPF) (García-Mayordomo et al., 2012).

The generation and propagation of deep-water waves toward the port were simulated using the NLSWE Tsunami-HySEA model, which generates boundary conditions for the Boussinesq (FUNWAVE) model (both will use the same high-resolution numerical grid. Figure 18 presents the results of a comparison between the numerical model that solves the NLSWE (Tsunami-HySEA) and the Boussinesq-type model (FUNWAVE). Okada's geometric parameters are described in Table 10.

Table 10. Okada's geometric parameters for simulated tsunami scenarios related to the Horse Shoe Fault (HSF) and the Marques de Pombal Fault (MPF).

Ref	Lon	Lat	Hypocenter (km)	Length (km)	Width (km)	Strike	Dip	Rake	Slip (m)
HSF + MPF	-10.32	35.92	33.678	170	100	42	35	90	14
	-10.25	36.64	27.943	120	80	20	35	90	12

The comparison suggests that, for the selected deterministic scenario, the differences between Tsunami-HySEA and FUNWAVE in maximum inundation depth and flooded extent are relatively small, generally within approximately 5%. Therefore, for the asset-oriented risk assessment developed here, these differences are unlikely to substantially modify the resulting TIM-based damage-state assignments.

https://doi.org/10.5194/egusphere-2026-4720
Preprint. Discussion started: 14 August 2026
© Author(s) 2026. CC BY 4.0 License.

For the purpose of the asset-oriented risk assessment proposed in this study, these differences are considered negligible, as neither harbour resonance nor frequency-dispersion effects significantly modify the overland inundation patterns from which the TIMs and subsequent risk measures are derived. Therefore, the NLSWE formulation provides an appropriate balance between physical realism and computational efficiency for probabilistic tsunami-risk assessments requiring thousands of simulations.

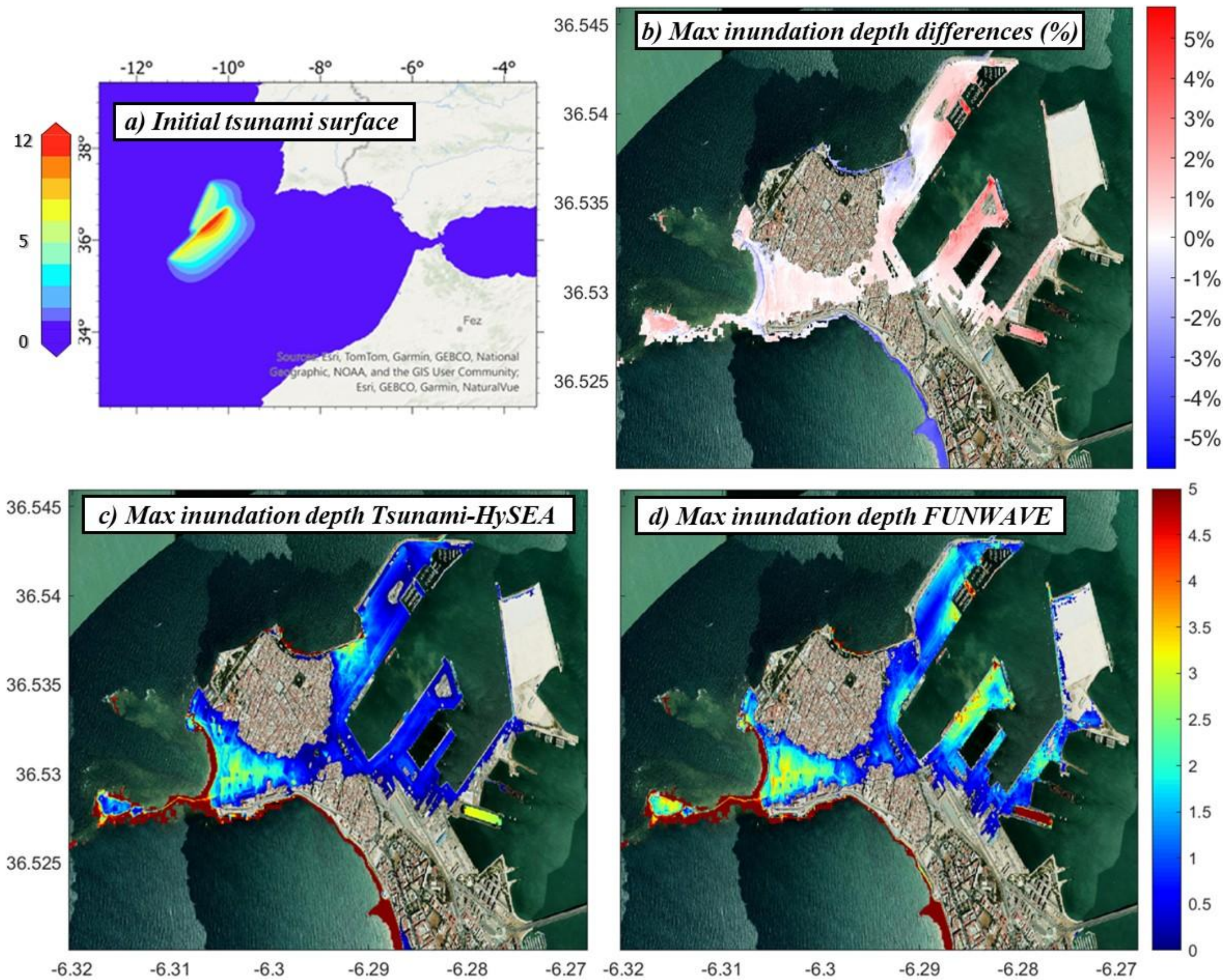

Figure 18. The upper left panel shows the initial tsunami run-up generated by the combined activity of the Horse Shoe and Marqués de Pombal faults. The lower panel shows maps of the maximum inundation depth resulting from the tsunami simulated using the Tsunami-HySEA model (NLSWE) on the left and the FUNWAVE model (BOUSSINESQ) on the right. The upper right plot presents the relative differences between the two models, expressed as percentages. The base map in a) was designed and developed by Esri | Powered by Esri. Base maps sources for b), c) and d): © Plan Nacional de Ortofotografía Aérea (PNOA) - Instituto Geográfico Nacional. Spain, 2025.

https://doi.org/10.5194/egusphere-2026-4720
Preprint. Discussion started: 14 August 2026
© Author(s) 2026. CC BY 4.0 License.

In addition, it should be noted that present analysis is carried out under a fixed sea-level condition, it is important to acknowledge that tidal variability represents an additional source of uncertainty in tsunami hazard and risk assessments. The tidal stage at the time of tsunami arrival can influence the extent and inundation depth. From a probabilistic perspective, the occurrence of a tsunami and the tidal stage at the time of impact are independent processes, and their combined effect can therefore be considered through their joint probability within a PTHA framework.

In practical applications, adopting a representative sea level such as mean sea level can be interpreted as an intermediate condition that provides a simplified yet physically meaningful approximation of tsunami impact. However, this approach implicitly assumes a deterministic boundary that does not fully reflect the natural variability of coastal systems. Incorporating tidal variability as a probabilistic variable within hazard and risk frameworks would allow for a more comprehensive representation of potential impact scenarios. This aspect remains an important challenge and consideration for future developments in tsunami risk assessment.

The proposed methodology fills an existing gap in the literature regarding the detailed analysis of the port landside operational area, enabling the transition from physical hazard to the estimation of the state of structural damage. The present study highlights the effort to synthesize empirical damage studies on key port assets (Cargo Handling equipment, warehouses, buildings, containers, tanks, vehicles and other Ro-Ro, and areas for pedestrian traffic). Although much of the existing literature focuses on inundation depth as the dominant variable, the results reinforce the need to consider flow velocity and associated hydrodynamic loads as critical damage variables, especially for large, highly exposed assets.

Despite the limitations related to knowledge of the vulnerability of assets to tsunami impacts, this study lays the groundwork for port management that integrates tsunamis into the strategic planning of the maritime sector. One of the main technical advancements of this framework lies in the explicit formulation of different damage state functions and thresholds for tsunami intensity measures (TIM), tailored to the physical characteristics of each asset.

However, the approach has limitations inherent to the use of discrete scales and the ordinal nature of the indices used. The definition of thresholds involves a certain degree of subjectivity, the dimensionless nature of the index limits its quantitative interpretation, and nonlinear interactions between hydrodynamic variables are not explicitly represented. While acknowledging its limitations, the proposed methodology provides an adaptable basis for future developments and applications in ports exposed to tsunamis. The main limitations of the methodology arise from the fact that the resulting risk index cannot be interpreted as an absolute measure of expected damage or loss. Nevertheless, within the context of strategic tsunami-risk analysis in ports, the proposed methodology is considered robust, consistent and aligned with established practices in natural-hazard risk assessment.

Future research should focus on developing asset-specific vulnerability functions, jointly incorporating flow depth and velocity, and integrating more advanced probabilistic approaches to reduce uncertainty in the interaction between different elements (debris). Another challenge for future research is the need to extend the analysis beyond direct physical damage. A

https://doi.org/10.5194/egusphere-2026-4720
Preprint. Discussion started: 14 August 2026
© Author(s) 2026. CC BY 4.0 License.

comprehensive risk assessment in ports must consider indirect damage and the spread of consequences throughout the supply chain, with business continuity models and network analytics (like Chua et al., 2024), allowing the quantification of how the failure in a component of the landside operational area propagates, affecting the overall operation of the port.

Finally, it is important to recognise that tsunami impacts extend beyond direct physical damage. In port environments, primary structural failures may trigger cascading technological accidents (NaTech events), leading to secondary hazards that complicate emergency response, operability, and long-term environmental recovery. Moreover, more refined vulnerability assessments for people in port areas would require consideration of individual characteristics (e.g. age, weight, height, mobility) and site-specific conditions, such as enclosed versus open spaces, debris presence, and evacuation planning availability.

8. Conclusions

This study developed and applied a methodological framework for tsunami risk assessment in the landside operational areas of port facilities. The framework integrates tsunami hazard, exposure, and asset-specific vulnerability information within a spatially explicit structure designed to support the assessment of direct physical impacts on port assets. By considering the multi-asset nature of port environments, the proposed approach provides a structured basis for analysing how tsunami-induced inundation may affect critical assets of port operations.

The framework is organised around four main components. The port characterization is derived from the port setting and involves identifying the relevant physical assets and cargo. These are represented geospatially with attributes such as type, use, and throughput statistics. The tsunami hazard assessment provides the hydrodynamic input required to characterise the intensity of the event within the port domain, expressed through Tsunami Intensity Measures (TIMs). The exposure assessment identifies and spatially represents the assets, goods, and people located within the potentially affected areas, distinguishing between static and dynamic exposure conditions. The vulnerability assessment translates the selected TIMs damage using asset-specific damage state functions derived for distinct assets typologies. Finally, the risk assessment integrates these components through two complementary outputs: a specific-impact assessment at asset scale and a dock-level Integrated Risk Index (IRI^{dock}).

The comparison between Tsunami-HySEA and FUNWAVE demonstrated only minor differences in the predicted overland inundation extent. Although larger discrepancies may arise within harbour basins due to resonance and wave-dispersion effects, these differences have a negligible influence on the land inundation patterns governing the TIMs used in the proposed risk assessment. Consequently, for the asset-oriented probabilistic framework developed in this study, the NLSWE provide an appropriate balance between physical realism and computational efficiency, enabling large-scale probabilistic tsunami risk assessments requiring thousands of numerical simulations without compromising the reliability of the estimated damage and risk metrics.

https://doi.org/10.5194/egusphere-2026-4720
Preprint. Discussion started: 14 August 2026
© Author(s) 2026. CC BY 4.0 License.

The application of the framework to the Port of Cádiz illustrates its practical value for analysing tsunami risk in a real port environment. The methodology used NEAMTHM18 products, enabling probabilistic that include the epistemic uncertainty of hydrodynamic variables that can be directly used for damage assessment. The methodology allowed for the identification of spatial differences in risk among docks and asset categories, showing how the combination of hazard intensity, exposure distribution, and asset-specific vulnerability can reveal impact patterns that would not be captured by hazard maps alone. The case study also demonstrates the relevance of considering different types of assets, including cargo-handling equipment, storage facilities, tanks, containers, vehicles, Ro-Ro areas, and pedestrian zones, since each of them may respond differently to the same hydrodynamic conditions.

The first main output of the framework is the specific-impact assessment, which allows the identification of exposed assets that may reach predefined damage states under a given tsunami scenario. This result is particularly useful for recognizing critical assets and locating areas where specific physical impacts may occur. The second main output is the Integrated Risk Index at dock scale (IRI^{dock}). The IRI^{dock} provides a spatially aggregated representation of relative risk levels across the port, enabling comparison among docks or operational sections. This index is useful for identifying areas where the concentration of exposed assets and their expected damage states may lead to comparatively higher risk levels. However, it should be emphasized that the IRI^{dock} is a relative and comparative indicator. It does not represent an absolute estimate of physical damage, economic loss, downtime, or probability of failure. Rather, it is intended as a decision-support measure for prioritizing areas within the port that may require further assessment, mitigation, preparedness, or contingency planning.

The framework is transferable to other port contexts, provided that suitable local information is available. The methodology should not be interpreted as a universal set of fixed thresholds, but rather as a flexible assessment framework that can be adjusted to different port layouts, tsunamigenic settings, asset typologies, and data availability levels.

Overall, the proposed framework contributes to bridging tsunami hazard modelling and port risk-management practice by providing a procedure to translate hydrodynamic outputs into asset-level damage information and relative dock-level risk indicators. While further refinement and validation are needed, the present methodology offers a practical and transferable basis for supporting tsunami risk assessment, spatial prioritisation, and resilience planning in port environments.

9. Code availability

The tsunami numerical code FUNWAVE-TVD is available on the GitHub website (https://github.com/fengyanshi/FUNWAVE-TVD). The tsunami numerical code Tsunami-HySEA model is available on the GitHub website (https://github.com/edanya-uma/Tsunami-HySEA).

https://doi.org/10.5194/egusphere-2026-4720
Preprint. Discussion started: 14 August 2026
© Author(s) 2026. CC BY 4.0 License.

10. Data availability

The NEAMTHM18 data and results are available on the website (https://www.tsumaps-neam.eu/tsunami-hazard/neamthm18). The bathymetric GEBCO data can be obtained from (https://download.gebco.net/). The EMODnet database can be obtained from (https://emodnet.ec.europa.eu/en/data-0). The supplemented nautical charts and a detailed bathymetric survey and the Port planimetry can be obtained from the local port authority.

11. Author contribution

SP, IA-A, MG and IA-Q developed the methodology and reviewed and edited the manuscript. MG supervised the research and reviewed and edited the manuscript. DGP performed the tsunami numerical simulations. All authors discussed the results and approved the final version of the manuscript.

12. Competing interests

Some authors are members of the editorial board of the journal.

13. Acknowledgements

The authors gratefully acknowledge Puertos del Estado and the Port Authority of the Bay of Cádiz for providing the data and information related to the Port of Cádiz terminal. Computational resources were provided through access to the Leonardo supercomputer at CINECA, granted by the Italian National Institute of Geophysics and Volcanology (INGV).

14. Financial support

Financial support for this research was provided by the TSUPORT project (grant PID2023-151688OA-I00), funded by the Spanish Ministry of Science, Innovation and Universities, Spain's State Research Agency (AEI) and the European Regional Development Fund (FEDER), EU. The lead author gratefully acknowledges the financial support received from the Spanish Ministry of Science, Innovation, and Universities through the FPU predoctoral fellowship FPU21/05272.

15. References

Abson, D. J., Dougill, A. J., and Stringer, L. C.: Using Principal Component Analysis for information-rich socio-ecological vulnerability mapping in Southern Africa, Applied Geography, 35, 515–524, https://doi.org/10.1016/j.apgeog.2012.08.004, 2012.

Aguirre-Ayerbe, I., Martínez Sánchez, J., Aniel-Quiroga, Í., González-Riancho, P., Merino, M., Al-Yahyai, S., González, M., and Medina, R.: From tsunami risk assessment to disaster risk reduction-the case of Oman, Hazards Earth Syst. Sci, 18, 2241–2260, https://doi.org/10.5194/nhess-18-2241-2018, 2018.

Aguirre-Ayerbe, I., Galán Pérez, D., Merino, M., and González Rodríguez, E. M.: Tsunami Hazard Map for Cádiz (Spain) derived from a Local-Scale Probabilistic Tsunami Hazard Assessment (S-PTHA) and Science-Based Participatory Decision-Making, https://doi.org/10.5281/zenodo.17432571, 2025.

Al-Qadami, E., Razi, M. A. M., Shah, S. M. H., Pu, J. H., Amran, M., Díaz Huenchuan, M. A., and Avudaiappan, S.: Floodwaters and vehicle hydrodynamics: A deep dive into risk mitigation unraveling vehicle stability in floods, Results in Engineering, 23, 102540, https://doi.org/10.1016/j.rineng.2024.102540, 2024.

Al-Qadami, E. H. H., Mustaffa, Z., Shah, S. M. H., Matínez-Gomariz, E., and Yusof, K. W.: Full-scale experimental investigations on the response of a flooded passenger vehicle under subcritical conditions, Natural Hazards, 110, 325–348, https://doi.org/10.1007/s11069-021-04949-6, 2022.

Álvarez-Gómez, J. A., Aniel-Quiroga, Í., Gutiérrez-Gutiérrez, O. Q. Q., Larreynaga, J., González, M., Castro, M., Gavidia, F., Aguirre-Ayerbe, I., González-Riancho, P., and Carreño, E.: Tsunami hazard assessment in El Salvador, Central America, from seismic sources through flooding numerical models., Natural Hazards and Earth System Sciences, 13, 2927–2939, https://doi.org/10.5194/nhess-13-2927-2013, 2013.

Aniel-Quiroga, Í., Quetzalcóatl, O., González, M., and Guillou, L.: Tsunami run-up estimation based on a hybrid numerical flume and a parameterization of real topobathymetric profiles, Natural Hazards and Earth System Sciences, 18, 1469–1491, https://doi.org/10.5194/nhess-18-1469-2018, 2018.

Aranguiz, R., Catalán, P. A., Cecioni, C., Bellotti, G., Henriquez, P., and González, J.: Tsunami Resonance and Spatial Pattern of Natural Oscillation Modes With Multiple Resonators, J. Geophys. Res. Oceans, 124, 7797–7816, https://doi.org/10.1029/2019JC015206, 2019.

Arcos, M. E. M. and LeVeque, R. J.: Validating Velocities in the GeoClaw Tsunami Model Using Observations near Hawaii from the 2011 Tohoku Tsunami, Pure Appl. Geophys., 172, 849–867, https://doi.org/10.1007/s00024-014-0980-y, 2015.

Argyroudis, S. ., Basco, A. ., Babič, A. ., Anastasiadis, A. ., Iervolino, I., Tsionis, Georgios., Schleiss, A. J. ., Salzano, E. ., Rodrigues, D. ., Pitilakis, K. ., Mignan, A. ., Matos, J. P. ., Karafagka, S. ., Kakderi, K. ., Giardini, D. ., Giannopoulos, G. ., Galbusera, L. ., Fotopoulou, S. ., Dolšek, M. ., Crowley, H. ., and Casotto, C. .: Guidelines for harmonized vulnerability and risk assessment for non-nuclear critical infrastructure: STREST Reference Report 3, Publications Office, Luxembourg:, 47 pp., https://doi.org/10.2788/10912, 2016.

Bacigalupe, M. C. and Hansz, J. R.: Breves apuntes sobre logística, logística internacional y transporte marítimo por contenedores. Análisis para el caso del Uruguay y el Puerto de Montevideo., Anuario del Área Socio-Jurídica, 151st February, 01–21, https://doi.org/10.26668/1688-5465_anuariosociojuridico/2023.v15i1.9190, 2023.

Basili, R., Brizuela, B., Herrero, A., Iqbal, S., Lorito, S., Maesano, F. E., Murphy, S., Perfetti, P., Romano, F., Scala, A., Selva, J., Taroni, M., Tiberti, M. M., Thio, H. K., Tonini, R., Volpe, M., Glimsdal, S., Harbitz, C. B., Løvholt, F., Baptista, M. A.,

https://doi.org/10.5194/egusphere-2026-4720
Preprint. Discussion started: 14 August 2026
© Author(s) 2026. CC BY 4.0 License.

Carrilho, F., Matias, L. M., Omira, R., Babeyko, A., Hoechner, A., Gurbuz, M., Pekcan, O., Yalçıner, A., Canals, M., Lastras, G., Agalos, A., Papadopoulos, G., Triantafyllou, I., Benchekroun, S., Jaouadi, H. A., Attafi, K., Abdallah, S. Ben, Bouallegue, A., Hamdi, H., and Oueslati, F.: NEAMTHM18 Documentation: the making of the TSUMAPS-NEAM Tsunami Hazard Model 2018, https://doi.org/10.5281/zenodo.3406625, 2019.

Basili, R., Brizuela, B., Herrero, A., Iqbal, S., Lorito, S., Maesano, F. E., Murphy, S., Perfetti, P., Romano, F., Scala, A., Selva, J., Taroni, M., Tiberti, M. M., Thio, H. K., Tonini, R., Volpe, M., Glimsdal, S., Harbitz, C. B., Løvholt, F., Baptista, M. A., Carrilho, F., Matias, L. M., Omira, R., Babeyko, A., Hoechner, A., Gürbüz, M., Pekcan, O., Yalçıner, A., Canals, M., Lastras, G., Agalos, A., Papadopoulos, G., Triantafyllou, I., Benchekroun, S., Agrebi Jaouadi, H., Ben Abdallah, S., Bouallegue, A., Hamdi, H., Oueslati, F., Amato, A., Armigliato, A., Behrens, J., Davies, G., Di Bucci, D., Dolce, M., Geist, E., Gonzalez Vida, J. M., González, M., Macías Sánchez, J., Meletti, C., Ozer Sozdinler, C., Pagani, M., Parsons, T., Polet, J., Power, W., Sørensen, M., and Zaytsev, A.: The Making of the NEAM Tsunami Hazard Model 2018 (NEAMTHM18), Front. Earth Sci. (Lausanne)., 8, 616594, https://doi.org/10.3389/feart.2020.616594, 2021.

Behrens, J. and Dias, F.: New computational methods in tsunami science, Philosophical Transactions of the Royal Society A: Mathematical, Physical and Engineering Sciences, 373, 20140382, https://doi.org/10.1098/rsta.2014.0382, 2015.

Behrens, J., Løvholt, F., Jalayer, F., Lorito, S., Salgado-Gálvez, M. A., Sørensen, M., Abadie, S., Aguirre-Ayerbe, I., Aniel-Quiroga, I., Babeyko, A., Baiguera, M., Basili, R., Belliazzi, S., Grezio, A., Johnson, K., Murphy, S., Paris, R., Rafliana, I., De Risi, R., Rossetto, T., Selva, J., Taroni, M., Del Zoppo, M., Armigliato, A., Bureš, V., Cech, P., Cecioni, C., Christodoulides, P., Davies, G., Dias, F., Bayraktar, H. B., González, M., Gritsevich, M., Guillas, S., Harbitz, C. B., Kânoğlu, U., Macías, J., Papadopoulos, G. A., Polet, J., Romano, F., Salamon, A., Scala, A., Stepinac, M., Tappin, D. R., Thio, H. K., Tonini, R., Triantafyllou, I., Ulrich, T., Varini, E., Volpe, M., and Vyhmeister, E.: Probabilistic Tsunami Hazard and Risk Analysis: A Review of Research Gaps, Front. Earth Sci. (Lausanne)., 9, 1–28, https://doi.org/10.3389/feart.2021.628772, 2021.

Berger, M. J., George, D. L., LeVeque, R. J., and Mandli, K. T.: The GeoClaw software for depth-averaged flows with adaptive refinement, Adv. Water Resour., 34, 1195–1206, https://doi.org/10.1016/J.ADVWATRES.2011.02.016, 2011.

Borrero, J. C., Lynett, P. J., and Kalligeris, N.: Tsunami currents in ports, Philosophical Transactions of the Royal Society A: Mathematical, Physical and Engineering Sciences, 373, 20140372, https://doi.org/10.1098/rsta.2014.0372, 2015.

Brocchini, M.: A reasoned overview on Boussinesq-type models: the interplay between physics, mathematics and numerics, Proceedings of the Royal Society A: Mathematical, Physical and Engineering Sciences, 469, 20130496, https://doi.org/10.1098/rspa.2013.0496, 2013.

Marinas Market Size, Share, Growth, and Industry Analysis: https://www.businessresearchinsights.com/market-reports/marinas-market-119327, last access: 12 June 2025.

CGS: https://storymaps.arcgis.com/stories/2bf182c1ae194ca29cd4c65f6ee47918, last access: 10 June 2025.

Cercone, C., Naito, C., Riggs, H. R., and Schellberg, R.: Quantifying Structural Impact Demands Due to Tsunami-Generated Debris, in: Structures Congress 2017, 169–182, https://doi.org/10.1061/9780784480427.015, 2017.

https://doi.org/10.5194/egusphere-2026-4720
Preprint. Discussion started: 14 August 2026
© Author(s) 2026. CC BY 4.0 License.

Charvet, I., Macabuag, J., and Rossetto, T.: Estimating Tsunami-Induced Building Damage through Fragility Functions: Critical Review and Research Needs, Front. Built Environ., 3, 3–36, https://doi.org/10.3389/fbuil.2017.00036, 2017.

Choi, Y.-K., Shi, F., Malej, M., Smith, J. M., Kirby, J. T., and Grilli, S. T.: Block-structured, equal-workload, multi-grid-nesting interface for the Boussinesq wave model FUNWAVE-TVD (Total Variation Diminishing), Geosci. Model Dev., 15, 5441–5459, https://doi.org/10.5194/gmd-15-5441-2022, 2022.

Chua, C. T., Switzer, A. D., Suppasri, A., Li, L., Pakoksung, K., Lallemant, D., Jenkins, S. F., Charvet, I., Chua, T., Cheong, A., and Winspear, N.: Tsunami damage to ports: cataloguing damage to create fragility functions from the 2011 Tohoku event, Natural Hazards and Earth System Sciences, 21, 1887–1908, https://doi.org/10.5194/nhess-21-1887-2021, 2021.

Chua, C. T., Otake, T., Li, T., Cheng, A.-C., Qiu, Q., Li, L., Suppasri, A., Imamura, F., and Switzer, A. D.: An approach to assessing tsunami risk to the global port network under rising sea levels, npj Natural Hazards, 1, 1–38, https://doi.org/10.1038/s44304-024-00039-2, 2024.

Cox, R. J., Shand, T. D., and Blacka, M. J.: Appropriate safety criteria for people, Barton ACT 2600, 22 pp., 2010.

Cruz, A. M., Krausmann, E., and Franchello, G.: Analysis of tsunami impact scenarios at an oil refinery, Natural Hazards, 58, 141–162, https://doi.org/10.1007/s11069-010-9655-x, 2011.

Dias, W. P. S. and Edirisooriya, U.: Derivation of tsunami damage curves from fragility functions, Natural Hazards, 96, 1153–1166, https://doi.org/10.1007/s11069-019-03601-8, 2019.

Dong, G., Zheng, Z., Gao, J., Ma, X., Dong, Y., and Wu, H.: Experimental investigation on special modes with narrow amplification diagrams in harbor oscillations, Coastal Engineering, 159, 103720, https://doi.org/10.1016/j.coastaleng.2020.103720, 2020.

Elkafas, A. G., Elgohary, M. M., and Zeid, A. E.: Numerical study on the hydrodynamic drag force of a container ship model, Alexandria Engineering Journal, 58, 849–859, https://doi.org/10.1016/j.aej.2019.07.004, 2019.

Ferrotto, M. F. and Cavaleri, L.: Masonry structures: A proposal of analytical generation of fragility functions for tsunami impact – Application to the Mediterranean coasts, Eng. Struct., 242, 112463, https://doi.org/10.1016/j.engstruct.2021.112463, 2021.

Supply Chain Management Review: https://www.scmr.com/article/the_role_of_maritime_ports_in_the_global_supply_chain_networks_of_automotiv, last access: 13 June 2025.

Fritz, H. M., Petroff, C. M., Catalán, P. A., Cienfuegos, R., Winckler, P., Kalligeris, N., Weiss, R., Barrientos, S. E., Meneses, G., Valderas-Bermejo, C., Ebeling, C., Papadopoulos, A., Contreras, M., Almar, R., Dominguez, J. C., and Synolakis, C. E.: Field Survey of the 27 February 2010 Chile Tsunami, Pure Appl. Geophys., 168, 1989–2010, https://doi.org/10.1007/s00024-011-0283-5, 2011.

Gao, J., Ma, X., Dong, G., Zang, J., Zhou, X., and Zhou, L.: Topographic influences on transient harbor oscillations excited by N-waves, Ocean Engineering, 192, 106548, https://doi.org/10.1016/J.OCEANENG.2019.106548, 2019.

https://doi.org/10.5194/egusphere-2026-4720
Preprint. Discussion started: 14 August 2026
© Author(s) 2026. CC BY 4.0 License.

Gao, L., Chen, Z., Yang, H., Wan, X., and Wang, M.: Hydrodynamic pressure law of ground-rested circular RC tank under bi-directional horizontal seismic action, PLoS One, 17, e0265528, https://doi.org/10.1371/JOURNAL.PONE.0265528, 2022.

García-Mayordomo, J., Insua-Arévalo, J. M., Martínez-Díaz, J. J., Jiménez-Díaz, A., Martín-Banda, R., Martín-Alfageme, S., Álvarez-Gómez, J. A., Rodríguez-Peces, M., Pérez-López, R., Rodríguez-Pascua, M. A., Masana, E., Perea, H., Martín-González, F., Giner-Robles, J., Nemser, E. S., and Cabral, J.: The Quaternary Active Faults Database of Iberia (QAFI v.2.0), Journal of Iberian Geology, 38, 285–302, https://doi.org/10.5209/rev_JIGE.2012.v38.n1.39219, 2012.

Garcia-Orellana, J., Gràcia, E., Vizcaino, A., Masqué, P., Olid, C., Martínez-Ruiz, F., Piñero, E., Sanchez-Cabeza, J., and Dañobeitia, J.: Identifying instrumental and historical earthquake records in the SW Iberian margin using 210Pb turbidite chronology, Geophys. Res. Lett., 33, 2–6, https://doi.org/10.1029/2006GL028417, 2006.

Gibbons, S. J., Lorito, S., Macías, J., Løvholt, F., Selva, J., Volpe, M., Sánchez-Linares, C., Babeyko, A., Brizuela, B., Cirella, A., Castro, M. J., de la Asunción, M., Lanucara, P., Glimsdal, S., Lorenzino, M. C., Nazaria, M., Pizzimenti, L., Romano, F., Scala, A., Tonini, R., Manuel González Vida, J., and Vöge, M.: Probabilistic Tsunami Hazard Analysis: High Performance Computing for Massive Scale Inundation Simulations, Front. Earth Sci. (Lausanne)., 8, 591549, https://doi.org/10.3389/feart.2020.591549, 2020.

Glimsdal, S., Løvholt, F., Harbitz, C. B., Romano, F., Lorito, S., Orefice, S., Brizuela, B., Selva, J., Hoechner, A., Volpe, M., Babeyko, A., Tonini, R., Wronna, M., and Omira, R.: A New Approximate Method for Quantifying Tsunami Maximum Inundation Height Probability, Pure Appl. Geophys., 176, 3227–3246, https://doi.org/10.1007/S00024-019-02091-W/FIGURES/17, 2019.

Goda, K. and De Risi, R.: Time-dependent probabilistic tsunami risk assessment: application to Tofino, British Columbia, Canada, subjected to Cascadia subduction earthquakes, npj Natural Hazards, 1, 7, https://doi.org/10.1038/s44304-024-00006-x, 2024.

González, A., Fernández, M., Llorente, M., Macías, J., Sánchez-Linares, C., García-Mayordomo, J., and Paredes, C.: Pseudo-Probabilistic Design for High-Resolution Tsunami Simulations in the Southwestern Spanish Coast, GeoHazards, 3, 294–322, https://doi.org/10.3390/geohazards3020016, 2022.

González, M., Álvarez-Gómez, J. A., Aniel-Quiroga, Í., Otero, L., Olabarrieta, M., Omira, R., Luceño, A., Jelinek, R., Krausmann, E., Birkman, J., Baptista, M. A., Miranda, M., and Aguirre-Ayerbe, I.: Probabilistic Tsunami Hazard Assessment in Meso and Macro Tidal Areas. Application to the Cádiz Bay, Spain, Front. Earth Sci. (Lausanne)., 9, https://doi.org/10.3389/feart.2021.591383, 2021.

González-Riancho, P., Aguirre-Ayerbe, I., García-Aguilar, O., Medina, R., González, M., Aniel-Quiroga, Í., Gutiérrez, O. Q., Álvarez-Gómez, J. A., Larreynaga, J., and Gavidia, F.: Integrated tsunami vulnerability and risk assessment: application to the coastal area of El Salvador, Natural Hazards and Earth System Science, 14, 1223–1244, https://doi.org/10.5194/nhess-14-1223-2014, 2014.

Goyo, Y.: TSUNAMI DAMAGE TO OIL STORAGE TANKS, in: The 14 th World Conference on Earthquake Engineering, 12-17october, 1–8, 2008.

https://doi.org/10.5194/egusphere-2026-4720
Preprint. Discussion started: 14 August 2026
© Author(s) 2026. CC BY 4.0 License.

Hatayama, K.: Damage to Oil Storage Tanks from the 2011 Mw 9.0 Tohoku-Oki Tsunami, Earthquake Spectra, 31, 1103–1124, https://doi.org/10.1193/050713EQS120M, 2015.

Hatayama, K.: Tsunami Damage to Oil Storage Tanks in the Mw 9.0 2011 Tohoku, Japan Earthquake, in: 16th World Conference on Earthquake Engineering, 141, https://doi.org/10.1115/PVP2015-45530, 2017.

He, L., Yamauchi, S., Kioka, W., and Takahashi, R.: DRIFT BEHAVIOR OF AUTOMOBILES IN TSUNAMI, 土木学会論文集 B3（海洋開発）, 70, I_325-I_330, https://doi.org/10.2208/JSCEJOE.70.I_325, 2014.

Heintz, J. A. and Robertson, I. N.: Design of Structures for Vertical Evacuation from Tsunamis, in: Solutions to Coastal Disasters 2008, 72–81, https://doi.org/10.1061/40978(313)7, 2008.

Horrillo, J., Wood, A., Kim, G. -B, and Parambath, A.: A simplified 3-D Navier-Stokes numerical model for landslide-tsunami: Application to the Gulf of Mexico, J. Geophys. Res. Oceans, 118, 6934–6950, https://doi.org/10.1002/2012JC008689, 2013.

Horspool, N. A. and Fraser, S.: An Analysis of Tsunami Impacts to Lifelines, GNS Science Consultancy Report 2016/22, Auckland, 76 pp., 2016.

Hou, Y., Nakamura, T., Cho, Y.-H., Mizutani, N., and Tomita, T.: Influence of Tsunami-Driven Shipping Containers' Layout on Their Motion, J. Mar. Sci. Eng., 10, 1911, https://doi.org/10.3390/jmse10121911, 2022.

Hwang, T., Kim, J., Lee, D.-H., and Lee, J.-C.: Location Tracking of Drifting Container by Solitary Wave Load Using a Motion Analysis Program, Journal of Ocean Engineering and Technology, 37, 158–163, https://doi.org/10.26748/KSOE.2023.023, 2023.

Imai, K., Inazumi, T., Emoto, K., Horie, T., Suzuki, A., Kudo, K., Ogawa, M., Noji, M., Mizuto, K., and Sasaki, T.: Tsunami Vulnerability Criteria for Fishery Port Facilities in Japan, Geosciences (Basel)., 9, 410, https://doi.org/10.3390/geosciences9100410, 2019.

Jelínek, R., Krausmann, E., González, M., Álvarez-Gómez, J. A., Birkmann, J., and Welle, T.: Approaches for tsunami risk assessment and application to the city of Cádiz, Spain, Natural Hazards, 60, 273–293, https://doi.org/10.1007/S11069-011-0009-0, 2011.

Kazama, M. and Noda, T.: Damage statistics (Summary of the 2011 off the Pacific Coast of Tohoku Earthquake damage), Soils and Foundations, 52, 780–792, https://doi.org/10.1016/j.sandf.2012.11.003, 2012.

Keen, A. S., Lynett, P. J., Eskijian, M. L., Ayca, A., and Wilson, R.: Monte Carlo–Based Approach to Estimating Fragility Curves of Floating Docks for Small Craft Marinas, J. Waterw. Port Coast. Ocean Eng., 143, https://doi.org/10.1061/(ASCE)WW.1943-5460.0000385, 2017.

Keen, A. S., Lynett, P. J., Eskijian, M. L., Ayca, A., and Wilson, R. I.: Probabilistic Estimates of Tsunami Risk for Small Craft Marinas, J. Waterw. Port Coast. Ocean Eng., 147, 04020047, https://doi.org/10.1061/(ASCE)WW.1943-5460.0000599/ASSET/D5D0C1DB-F2D4-4B31-81D7-8F652C3D5C81/ASSETS/IMAGES/LARGE/WWENG-1531F12.JPG, 2021.

https://doi.org/10.5194/egusphere-2026-4720
Preprint. Discussion started: 14 August 2026
© Author(s) 2026. CC BY 4.0 License.

Kelly, A., Dengler, L. A., Uslu, B., Barberopoulou, A., Yim, S. C., and Bergen, K. J.: Recent tsunami highlights need for awareness of tsunami duration, Eos, Transactions American Geophysical Union, 87, 566–567, https://doi.org/10.1029/2006EO500004, 2006.

Kim, D.-H., Lynett, P. J., and Socolofsky, S. A.: A depth-integrated model for weakly dispersive, turbulent, and rotational fluid flows, Ocean Model. (Oxf)., 27, 198–214, https://doi.org/10.1016/j.ocemod.2009.01.005, 2009.

Koshimura, S., Namegaya, Y., and Yanagisawa, H.: Tsunami Fragility — A New Measure to Identify Tsunami Damage —, Journal of Disaster Research, 4, 479–488, https://doi.org/10.20965/jdr.2009.p0479, 2009.

Kumagai, K.: Tsunami-induced Debris of Freight Containers due to the 2011 off the Pacific Coast of Tohoku Earthquake, Tohoku, 25 pp., 2013.

Lario, J., Zazo, C., Goy, J. L., Silva, P. G., Bardaji, T., Cabero, A., and Dabrio, C. J.: Holocene palaeotsunami catalogue of SW Iberia, Quaternary International, 242, 196–200, https://doi.org/10.1016/j.quaint.2011.01.036, 2011.

Lee, W.-D., Kim, T., Kim, J., Kim, S.-K., Oh, H., and Hwang, T.: Experimental Investigation on the Drift and Collision of Containers Induced by Tsunami Action on a Wave Absorbing Revetment, Journal of Ocean Engineering and Technology, 38, 282–293, https://doi.org/10.26748/KSOE.2024.070, 2024.

Lekkas, E. L., Andreadakis, E., Kostaki, I., and Kapourani, E.: A Proposal for a New Integrated Tsunami Intensity Scale (ITIS-2012), Bulletin of the Seismological Society of America, 103, 1493–1502, https://doi.org/10.1785/0120120099, 2013.

Lima, V. V., Miranda, J. M., Baptista, M. A., Catalão, J., Gonzalez, M., Otero, L., Olabarrieta, M., Álvarez-Gómez, J. A., and Carreño, E.: Impact of a 1755-like tsunami in Huelva, Spain, Natural Hazards and Earth System Sciences, 10, 139–148, https://doi.org/10.5194/nhess-10-139-2010, 2010.

Lomnitz, C.: Major Earthquakes of Chile: A Historical Survey, 1535-1960, Seismological Research Letters, 75, 368–378, https://doi.org/10.1785/gssrl.75.3.368, 2004.

Lynett, P. J., Gately, K., Wilson, R., Montoya, L., Arcas, D., Aytore, B., Bai, Y., Bricker, J. D., Castro, M. J., Cheung, K. F., David, C. G., Dogan, G. G., Escalante, C., González-Vida, J. M., Grilli, S. T., Heitmann, T. W., Horrillo, J., Kânoğlu, U., Kian, R., Kirby, J. T., Li, W., Macías, J., Nicolsky, D. J., Ortega, S., Pampell-Manis, A., Park, Y. S., Roeber, V., Sharghivand, N., Shelby, M., Shi, F., Tehranirad, B., Tolkova, E., Thio, H. K., Velioğlu, D., Yalçıner, A. C., Yamazaki, Y., Zaytsev, A., and Zhang, Y. J.: Inter-model analysis of tsunami-induced coastal currents, Ocean Model. (Oxf)., 114, 14–32, https://doi.org/10.1016/j.ocemod.2017.04.003, 2017.

Lynham, J., Noy, I., and Page, J.: The 1960 Tsunami in Hawaii: Long-Term Consequences of a Coastal Disaster, World Dev., 94, 106–118, https://doi.org/10.1016/J.WORLDDEV.2016.12.043, 2017.

Ma, X., Zheng, Z., Zhang, X., and Dong, G.: Numerical investigation on special modes with narrow amplification diagram in harbor oscillations, Ocean Dyn., 70, 1–19, https://doi.org/10.1007/s10236-019-01325-8, 2020.

Macabuag, J., Rossetto, T., Ioannou, I., and Eames, I.: Investigation of the Effect of Debris-Induced Damage for Constructing Tsunami Fragility Curves for Buildings, Geosciences (Basel)., 8, 117, https://doi.org/10.3390/geosciences8040117, 2018.

https://doi.org/10.5194/egusphere-2026-4720
Preprint. Discussion started: 14 August 2026
© Author(s) 2026. CC BY 4.0 License.

Macías, J., Castro, M. J., Ortega, S., Escalante, C., and González-Vida, J. M.: Performance Benchmarking of Tsunami-HySEA Model for NTHMP's Inundation Mapping Activities, Pure and Applied Geophysics 2017 174:8, 174, 3147–3183, https://doi.org/10.1007/S00024-017-1583-1, 2017.

Macías, J., Castro, M. J., and Escalante, C.: Performance assessment of the Tsunami-HySEA model for NTHMP tsunami currents benchmarking. Laboratory data, Coastal Engineering, 158, 103667, https://doi.org/10.1016/j.coastaleng.2020.103667, 2020a.

Macías, J., Castro, M. J., Ortega, S., and González-Vida, J. M.: Performance assessment of Tsunami-HySEA model for NTHMP tsunami currents benchmarking. Field cases, Ocean Model. (Oxf)., 152, 101645, https://doi.org/10.1016/j.ocemod.2020.101645, 2020b.

Marras, S. and Mandli, K. T.: Modeling and Simulation of Tsunami Impact: A Short Review of Recent Advances and Future Challenges, Geosciences (Basel)., 11, 1–19, https://doi.org/10.3390/geosciences11010005, 2020.

Martínez, J., Medina, R., Aguirre-Ayerbe, I., Pellón, E., Ramírez, M., Menéndez, P., Casal, C., Cánovas, V., Delgado, D., Jiménez, J., and Suarez, G.: Coastal Disaster Risk Profile and Adaptation Recommendations Considering Climate Change Scenarios for Belize, Inter-American Development Bank, Washington, D. C., https://doi.org/10.18235/0004181, 2022.

Martínez-Gomariz, E., Gómez, M., and Russo, B.: Experimental study of the stability of pedestrians exposed to urban pluvial flooding, Natural Hazards, 82, 1259–1278, https://doi.org/10.1007/s11069-016-2242-z, 2016.

Martínez-Gomariz, E., Gómez, M., Russo, B., and Djordjević, S.: Stability criteria for flooded vehicles: a state-of-the-art review, J. Flood Risk Manag., 11, 817–826, https://doi.org/10.1111/jfr3.12262, 2018.

Martínez-Gomariz, E., Gómez, M., and Russo, B.: Estabilidad de vehículos frente a inundaciones: estudio numérico-experimental, Ribagua, 6, 123–137, https://doi.org/10.1080/23863781.2019.1685921, 2019a.

Martínez-Gomariz, E., Locatelli, L., Guerrero, M., Russo, B., and Martínez, M.: Socio-Economic Potential Impacts Due to Urban Pluvial Floods in Badalona (Spain) in a Context of Climate Change, Water 2019, Vol. 11, Page 2658, 11, 2658, https://doi.org/10.3390/W11122658, 2019b.

Martínez-Gomariz, E., Forero-Ortiz, E., Guerrero-Hidalga, M., Castán, S., and Gómez, M.: Flood Depth–Damage Curves for Spanish Urban Areas, Sustainability, 12, 1–25, https://doi.org/10.3390/su12072666, 2020.

Masina, M., Archetti, R., and Lamberti, A.: 21 may 2003 boumerdès earthquake: Numerical investigations of the rupture mechanism effects on the induced tsunami and its impact in harbors, J. Mar. Sci. Eng., 8, 1–48, https://doi.org/10.3390/jmse8110933, 2020.

McCabe, M., Stansby, P. K., Rogers, B. D., and Cunningham, L. S.: Boussinesq modelling of tsunami and storm wave impact, Proceedings of the Institution of Civil Engineers - Engineering and Computational Mechanics, 167, 106–116, https://doi.org/10.1680/eacm.13.00025, 2014.

Muhari, A., Imamura, F., Koshimura, S., and Post, J.: Examination of three practical run-up models for assessing tsunami impact on highly populated areas, Natural Hazards and Earth System Sciences, 11, 3107–3123, https://doi.org/10.5194/nhess-11-3107-2011, 2011.

https://doi.org/10.5194/egusphere-2026-4720
Preprint. Discussion started: 14 August 2026
© Author(s) 2026. CC BY 4.0 License.

Muhari, A., Charvet, I., Tsuyoshi, F., Suppasri, A., and Imamura, F.: Assessment of tsunami hazards in ports and their impact on marine vessels derived from tsunami models and the observed damage data, Natural Hazards, 78, 1309–1328, https://doi.org/10.1007/s11069-015-1772-0, 2015.

Mustaffa, Z., Hamid Hussein Al-Qadami, E., Muzzamil Hussain Shah, S., and Wan Yusof, K.: Impact and Mitigation Strategies for Flash Floods Occurrence towards Vehicle Instabilities, in: Flood Impact Mitigation and Resilience Enhancement, edited by: Huang, G., IntechOpen, 19, https://doi.org/10.5772/intechopen.92731, 2020.

Nagi, A., Schroeder, M., and Kersten, W.: Risk Management in Seaports: A Community Analysis at the Port of Hamburg, Sustainability, 13, 8035, https://doi.org/10.3390/su13148035, 2021.

Naito, C., Cox, D., Yu, Q.-S. "Kent," and Brooker, H.: Fuel Storage Container Performance during the 2011 Tohoku, Japan, Tsunami, Journal of Performance of Constructed Facilities, 27, 373–380, https://doi.org/10.1061/(ASCE)CF.1943-5509.0000339, 2013.

Nistor, I., Goseberg, N., and Stolle, J.: Tsunami-Driven Debris Motion and Loads: A Critical Review, Front. Built Environ., 3, 11, https://doi.org/10.3389/fbuil.2017.00002, 2017.

Notteboom, T., Pallis, A., and Rodrigue, J.-P.: Port Economics, Management and Policy, 1st ed., Routledge, London, https://doi.org/10.4324/9780429318184, 2021.

Nouri, Y., Nistor, I., Palermo, D., and Saatcioglu, M.: Tsunami-induced hydrodynamic and debris flow forces on structural elements, in: 9th Canadian Conference of Earthquake Engineering, 26-26 June, 2007.

Oda, K., Okamoto, O., and Kumagai, K.: Analysis of Spillover Process and Development of Estimation Methods of Tsunami Damage in Ports and Surrounding Areas, Tsukuba, 12 pp., 2007.

Okada, Y.: Surface deformation due to shear and tensile faults in a half-space, Bulletin of the Seismological Society of America, 75, 1135–1154, https://doi.org/10.1785/BSSA0750041135, 1985.

Padilla, S., Aniel-Quiroga, Í., Omira, R., González, M., Kim, J., and Baptista, M. A.: Volcano tsunamis and their effects on moored vessel safety: the 2022 Tonga event, Natural Hazards and Earth System Sciences, 24, 3095–3113, https://doi.org/10.5194/nhess-24-3095-2024, 2024.

Percher, M., Bruin, W., Dickenson, S., Eskijian, M., Oritatsu, Y., and Rudolph, R. W.: Performance of Port and Harbor Structures Impacted by the March 11, 2011 Great Tohoku Earthquake & Tsunami, in: Ports 2013, 610–619, https://doi.org/10.1061/9780784413067.063, 2013.

Percher, Marc.: Tohoku, Japan, Earthquake and Tsunami of 2011, 1st ed., edited by: Percher, M., American Society of Civil Engineers, Reston, VA, https://doi.org/10.1061/9780784413180, 2014.

Pilone, E. and Demichela, M.: A semi-quantitative methodology to evaluate the main local territorial risks and their interactions, Land use policy, 77, 143–154, https://doi.org/10.1016/J.LANDUSEPOL.2018.05.027, 2018.

Popovich, B., Wotherspoon, L., and Borrero, J.: An assessment of subduction zone-generated tsunami hazards in New Zealand Ports, Natural Hazards, 107, 171–193, https://doi.org/10.1007/s11069-021-04578-z, 2021.

Power, W., Wang, X., Wallace, L., Clark, K., and Mueller, C.: The New Zealand Probabilistic Tsunami Hazard Model: Development and implementation of a methodology for estimating tsunami hazard nationwide, Geol. Soc. Spec. Publ., 456, 199–217, https://doi.org/10.1144/SP456.6;SERIALTOPIC:TOPIC:SERIES-TYPE, 2018.

Puertos Del Estado: Recomendaciones del diseño y ejecución de las obras de abrigo: Parte 1ª — Bases y factores para el proyecto. Agentes climáticos (ROM 1.0-09)., primera ed., edited by: Puertos Del Estado, Puertos Del Estado, Madrid, 532 pp., 2009.

Puertos Del Estado: Recomendaciones para el proyecto y ejecución en Obras de Atraque y Amarre (ROM 2.0-11), I., edited by: Puertos Del Estado, Puertos Del Estado, Madrid, 2012.

Rafliana, I., Jalayer, F., Cerase, A., Cugliari, L., Baiguera, M., Salmanidou, D., Necmioğlu, Ö., Ayerbe, I. A., Lorito, S., Fraser, S., Løvholt, F., Babeyko, A., Salgado-Gálvez, M. A., Selva, J., De Risi, R., Sørensen, M. B., Behrens, J., Aniel-Quiroga, I., Del Zoppo, M., Belliazzi, S., Pranantyo, I. R., Amato, A., and Hancilar, U.: Tsunami risk communication and management: Contemporary gaps and challenges, International Journal of Disaster Risk Reduction, 70, 102771, https://doi.org/10.1016/J.IJDRR.2021.102771, 2022.

Reese, S., Bradley, B. A., Bind, J., Smart, G., Power, W., and Sturman, J.: Empirical building fragilities from observed damage in the 2009 South Pacific tsunami, Earth. Sci. Rev., 107, 156–173, https://doi.org/10.1016/j.earscirev.2011.01.009, 2011.

Rehman, K. and Cho, Y.-S.: Building Damage Assessment Using Scenario Based Tsunami Numerical Analysis and Fragility Curves, Water (Basel)., 8, 109, https://doi.org/10.3390/w8030109, 2016.

Robertson, I., Chock, G., and Morla, J.: Structural Analysis of Selected Failures Caused by the 27 February 2010 Chile Tsunami, Earthquake Spectra, 28, 215–243, https://doi.org/10.1193/1.4000035, 2012.

Roeber, V., Yamazaki, Y., and Cheung, K. F.: Resonance and impact of the 2009 Samoa tsunami around Tutuila, American Samoa, Geophys. Res. Lett., 37, https://doi.org/10.1029/2010GL044419, 2010.

Roig-Munar, F. X., Martín-Prieto, J. Á., Rodríguez-Perea, A., Ferrer, B. G., Manel, J., and Fernández, V.: MORFOMETRÍA Y DINÁMICA DE BLOQUES ASOCIADOS A TSUNAMI EN UNA RAMPA LITORAL DEL NORTE DE MENORCA (ILLES BALEARS), Revista de la Sociedad Geológica de España, 30, 2017.

Russo, B., Gómez, M., and Macchione, F.: Pedestrian hazard criteria for flooded urban areas, Natural Hazards, 69, 251–265, https://doi.org/10.1007/s11069-013-0702-2, 2013.

Russo, B., Velasco, M., Locatelli, L., Sunyer, D., Yubero, D., Monjo, R., Martínez-Gomariz, E., Forero-Ortiz, E., Sánchez-Muñoz, D., Evans, B., and Gómez, A. G.: Assessment of Urban Flood Resilience in Barcelona for Current and Future Scenarios. The RESCCUE Project, Sustainability 2020, Vol. 12, Page 5638, 12, 5638, https://doi.org/10.3390/SU12145638, 2020.

Selva, J., Tonini, R., Molinari, I., Tiberti, M. M., Romano, F., Grezio, A., Melini, D., Piatanesi, A., Basili, R., and Lorito, S.: Quantification of source uncertainties in Seismic Probabilistic Tsunami Hazard Analysis (SPTHA), Geophys. J. Int., 205, 1780–1803, https://doi.org/10.1093/GJI/GGW107, 2016.

Shah, S. M. H., Mustaffa, Z., and Yusof, K. W.: Impact of hydrodynamic forces on a static vehicle at varying Froude numbers under partial submergence and subcritical flow conditions, International Journal of Advanced and Applied Sciences, 6, 35–41, https://doi.org/10.21833/ijaas.2019.11.006, 2019.

Shah, S. M. H., Mustaffa, Z., Martinez-Gomariz, E., Kim, D. K., and Yusof, K. W.: Criterion of vehicle instability in floodwaters: past, present and future, International Journal of River Basin Management, 19, 1–23, https://doi.org/10.1080/15715124.2019.1566240, 2021.

Shand, T., Smith, G., Cox, R., and Blacka, M.: Development of Appropriate Criteria for the Safety and Stability of Persons and Vehicles in Floods, in: 34th IAHR World Congress. Balance and Uncertainty, 26 June - 1 July, 404–412, 2011.

Shi, F., Kirby, J. T., Harris, J. C., Geiman, J. D., and Grilli, S. T.: A high-order adaptive time-stepping TVD solver for Boussinesq modeling of breaking waves and coastal inundation, Ocean Model. (Oxf)., 43–44, 36–51, https://doi.org/10.1016/j.ocemod.2011.12.004, 2012.

Shoji, G. and Moriyama, T.: Evaluation of the Structural Fragility of a Bridge Structure Subjected to a Tsunami Wave Load, Journal of Natural Disaster Science, 29, 73–81, https://doi.org/10.2328/jnds.29.73, 2007.

Smith, G. P., Modra, B. D., Tucker, T. A., and Cox, R. J.: Vehicle stability testing for flood flows, Sidney, 53 pp., 2017.

Son, S., Lynett, P. J., and Kim, D.-H.: Nested and multi-physics modeling of tsunami evolution from generation to inundation, Ocean Model. (Oxf)., 38, 96–113, https://doi.org/10.1016/j.ocemod.2011.02.007, 2011.

Song, J., De Risi, R., and Goda, K.: Influence of flow velocity on tsunami loss estimation, Geosciences (Switzerland), 7, https://doi.org/10.3390/geosciences7040114, 2017.

Suppasri, A., Koshimura, S., Imai, K., Mas, E., Gokon, H., Muhari, A., and Imamura, F.: Damage Characteristic and Field Survey of the 2011 Great East Japan Tsunami in Miyagi Prefecture, Coastal Engineering Journal, 54, 1250005, https://doi.org/10.1142/S0578563412500052, 2012.

Suppasri, A., Mas, E., Charvet, I., Gunasekera, R., Imai, K., Fukutani, Y., Abe, Y., and Imamura, F.: Building damage characteristics based on surveyed data and fragility curves of the 2011 Great East Japan tsunami, Natural Hazards, 66, 319–341, https://doi.org/10.1007/s11069-012-0487-8, 2013.

Suppasri, A., Charvet, I., Imai, K., and Imamura, F.: Fragility Curves Based on Data from the 2011 Tohoku-Oki Tsunami in Ishinomaki City, with Discussion of Parameters Influencing Building Damage, Earthquake Spectra, 31, 841–868, https://doi.org/10.1193/053013EQS138M, 2015.

Suppasri, A., Pakoksung, K., Charvet, I., Ting Chua, C., Takahashi, N., Ornthammarath, T., Latcharote, P., Leelawat, N., and Imamura, F.: Load-resistance analysis: An alternative approach to tsunami damage assessment applied to the 2011 Great East Japan tsunami, Natural Hazards and Earth System Sciences, 19, 1807–1822, https://doi.org/10.5194/NHESS-19-1807-2019, 2019.

Suppasri, A., Nishida, T., Pakoksung, K., Cheng, A. C., Chua, C. T., Iwasaki, T., Pescaroli, G., and Imamura, F.: Quantifying tsunami impact on industrial facilities and production capacity in ports: An application to Sendai Port, Japan, International Journal of Disaster Risk Reduction, 78, 103141, https://doi.org/10.1016/j.ijdrr.2022.103141, 2022.

https://doi.org/10.5194/egusphere-2026-4720
Preprint. Discussion started: 14 August 2026
© Author(s) 2026. CC BY 4.0 License.

Synolakis, C. E. and Kong, L.: Runup Measurements of the December 2004 Indian Ocean Tsunami, Earthquake Spectra, 22, 67–91, https://doi.org/10.1193/1.2218371, 2006.

Takahashi, S., Molenaar, W., Tomita, T., Burcharth, H. F., Headland, J. R., Memos, C. D., Diposaptono, S., Hettiarachchi, S. S. L., Lukkunaprasit, P., Yalciner, A. C., Yim, S., Montoya, J. M., Arikawa, T., Samarawickrama, S., and Rasch, P. S.: Mitigation of Tsunami Disasters in Ports, Belgique, 2010.

Takahashi, S., Honda, K., Nosu, A., Kawai, H., Takagawa, T., Tomita, T., Yeom, G., Asai, T., Okamoto, O., Kumagai, K., Kuriyama, Y., Fujita, I., Sugano, T., Arikawa, T., Shimosako, K., and Takata, N.: Tsunami Disasters in Ports due to the Great East Japan Earthquake, Pianc, Bruxelles, 2014.

Tang, A., Ames, D., McLaughlin, J., Murugesh, G., Plant, G., Yashinsky, M., Eskijian, M., Surrampalli, R., Murthy, P. A. K., Prasad, M., and Gandhi, P.: Coastal Indian Lifelines after the 2004 Great Sumatra Earthquake and Indian Ocean Tsunami, Earthquake Spectra, 22, S607–S639, https://doi.org/10.1193/1.2206089, 2006.

Tarbotton, C., Dall'Osso, F., Dominey-Howes, D., and Goff, J.: The use of empirical vulnerability functions to assess the response of buildings to tsunami impact: Comparative review and summary of best practice, Earth. Sci. Rev., 142, 120–134, https://doi.org/10.1016/J.EARSCIREV.2015.01.002, 2015.

Aftershocks shake Japan's auto industry: https://money.cnn.com/2011/03/14/autos/japan_autos_earthquake.fortune/index.htm, last access: 13 June 2025.

Tomita, T., Arikawa, T., and Asai, T.: Damage in Ports due to the 2011 off the Pacific Coast of Tohoku Earthquake Tsunami, Journal of Disaster Research, 8, 594–604, https://doi.org/10.20965/jdr.2013.p0594, 2013.

Tonini, R., Di Manna, P., Lorito, S., Selva, J., Volpe, M., Romano, F., Basili, R., Brizuela, B., Castro, M. J., de la Asunción, M., Di Bucci, D., Dolce, M., Garcia, A., Gibbons, S. J., Glimsdal, S., González-Vida, J. M., Løvholt, F., Macías, J., Piatanesi, A., Pizzimenti, L., Sánchez-Linares, C., and Vittori, E.: Testing Tsunami Inundation Maps for Evacuation Planning in Italy, Front. Earth Sci. (Lausanne)., 9, 1–19, https://doi.org/10.3389/feart.2021.628061, 2021.

Tran, Q. H., Huh, J., Doan, N. S., Van Mac, H., and Ahn, J. H.: Fragility Assessment of a Container Crane under Seismic Excitation Considering Uplift and Derailment Behavior, Applied Sciences 2019, Vol. 9, Page 4660, 9, 4660, https://doi.org/10.3390/APP9214660, 2019.

UAB: https://uab-online.com/news/what-is-liquid-bulk-cargo, last access: 20 June 2025.

UNDRR: https://www.undrr.org/terminology/disaster-risk-assessment, last access: 17 December 2025.

Valencia, N., Gardi, A., Gauraz, A., Leone, F., and Guillande, R.: New tsunami damage functions developed in the framework of SCHEMA project: application to European-Mediterranean coasts, Natural Hazards and Earth System Sciences, 11, 2835–2846, https://doi.org/10.5194/nhess-11-2835-2011, 2011.

Vela, J., Pérez, B., González, M., Otero, L., Olabarrieta, M., Canals, M., and Casamor, J. L.: Tsunami Resonance in Palma Bay and Harbor, Majorca Island, as Induced by the 2003 Western Mediterranean Earthquake, J. Geol., 122, 165–182, https://doi.org/10.1086/675256, 2014.

https://doi.org/10.5194/egusphere-2026-4720
Preprint. Discussion started: 14 August 2026
© Author(s) 2026. CC BY 4.0 License.

Vitale, A., Ricci, F., Baltzopoulos, G., Cozzani, V., and Iervolino, I.: Risk Assessment of Oil Storage Facilities Exposed to Tsunami Hazard, Chem. Eng. Trans., 111, 163–168, https://doi.org/10.3303/CET24111028, 2024.

Wang, X.: COMCOT User Manual Ver. 1.7, Cornell University, 6, 1–59, 2009.

Wannous, C. and Velasquez, G.: United Nations Office for Disaster Risk Reduction (UNISDR)—UNISDR's Contribution to Science and Technology for Disaster Risk Reduction and the Role of the International Consortium on Landslides (ICL), in: Advancing Culture of Living with Landslides, edited by: Sassa, K., Miko, M., and Yin, Y., Springer International Publishing, Cham, 109–115, https://doi.org/10.1007/978-3-319-59469-9_6, 2017.

Watts, P., Grilli, S. T., Kirby, J. T., Fryer, G. J., and Tappin, D. R.: Landslide tsunami case studies using a Boussinesq model and a fully nonlinear tsunami generation model, Natural Hazards and Earth System Sciences, 3, 391–402, https://doi.org/10.5194/nhess-3-391-2003, 2003.

Williams, J. H., Wilson, T. M., Horspool, N., Lane, E. M., Hughes, M. W., Davies, T., Le, L., and Scheele, F.: Tsunami impact assessment: development of vulnerability matrix for critical infrastructure and application to Christchurch, New Zealand, Natural Hazards, 96, 1167–1211, https://doi.org/10.1007/s11069-019-03603-6, 2019.

Wilson, R., Lynett, P., Eskijian, M., Miller, K., LaDuke, Y., Curtis, E., Hornick, M., Keen, A., and Ayca, A.: Tsunami Hazard Analysis and Products for Harbors in California, in: Annual Meeting, 23 october, 9, https://doi.org/10.1130/abs/2017AM-306344, 2017.

Wilson, R. I., Admire, A. R., Borrero, J. C., Dengler, L. A., Legg, M. R., Lynett, P., McCrink, T. P., Miller, K. M., Ritchie, A., Sterling, K., and Whitmore, P. M.: Observations and Impacts from the 2010 Chilean and 2011 Japanese Tsunamis in California (USA), Pure Appl. Geophys., 170, 1127–1147, https://doi.org/10.1007/s00024-012-0527-z, 2013.

World Bank: The Container Port Performance Index 2022: A Comparable Assessment of Performance Based on Vessel Time in Port, World Bank, World Bank, 80 pp., https://doi.org/10.1596/39824, 2023.

Yalciner, A. C. and Pelinovsky, E. N.: A short cut numerical method for determination of periods of free oscillations for basins with irregular geometry and bathymetry, Ocean Engineering, 34, 747–757, https://doi.org/10.1016/j.oceaneng.2006.05.016, 2007.

Yamamoto, Y., Kozono, Y., Mas, E., Murase, F., Nishioka, Y., Okinaga, T., and Takeda, M.: Applicability of Calculation Formulae of Impact Force by Tsunami Driftage, J. Mar. Sci. Eng., 9, 20, https://doi.org/10.3390/jmse9050493, 2021.

Yamazaki, Y. and Cheung, K. F.: Shelf resonance and impact of near-field tsunami generated by the 2010 Chile earthquake, Geophys. Res. Lett., 38, 1–8, https://doi.org/10.1029/2011GL047508, 2011.

Yeh, H., Yeh, H., Barbosa, A. R., Ko, H., and Cawley, J. G.: TSUNAMI LOADINGS ON STRUCTURES: REVIEW AND ANALYSIS, Coastal Engineering Proceedings, 1, currents.4, https://doi.org/10.9753/icce.v34.currents.4, 2014.

Yoshida, S.: Earthquake Damages and Disaster Prevention of Aboveground Storage Tanks, EPI International Journal of Engineering, 1, 87–93, https://doi.org/10.25042/epi-ije.082018.14, 2018.

Yuan, Y., Shi, F., Kirby, J. T., and Yu, F.: FUNWAVE-GPU: Multiple-GPU Acceleration of a Boussinesq-Type Wave Model, J. Adv. Model. Earth Syst., 12, e2019MS001957, https://doi.org/10.1029/2019MS001957, 2020.

https://doi.org/10.5194/egusphere-2026-4720
Preprint. Discussion started: 14 August 2026
© Author(s) 2026. CC BY 4.0 License.

Zhang, Y. J., Ye, F., Stanev, E. V., and Grashorn, S.: Seamless cross-scale modeling with SCHISM, Ocean Model. (Oxf)., 102, 64–81, https://doi.org/10.1016/j.ocemod.2016.05.002, 2016.